Structures 73 (2025) 108361

Contents lists available at ScienceDirect

Structures

journal homepage: www.elsevier.com/locate/structures

Experimental and numerical study for flexural behavior of RC two-way slabs with openings strengthened by EBR and NSM techniques

Mohamed AbdelBaset, Mohamed H. Makhlouf *, Marwa H. Bondok, Gamal I. Khaleel

Civil Department, Benha Faculty of Engineering, Benha University, Egypt

ARTICLE INFO

Keywords:
Two-way RC slabs
Openings
Externally bounded glass fiber-reinforced polymer (EB-GFRP)
Near surface-mounted technique (NSM)
ABAQUS

ABSTRACT

Openings in existing two-way R.C. slabs are frequently created as a result of delayed design needs. While allowed under some circumstances, this practice can result in a weakened slab and decrease its ability to bear weight, as it creates a discontinuity in the reinforcing bars. This research aims to examine the flexural behavior of two-way R. C. slabs with an opening. The parameters of the study included the surface area, the number of layers of glass fiber-reinforced polymer (GFRP) sheets, and the method of strengthening, which involved a combination of externally bonded reinforcement (EBR) and near-surface mounted (NSM) strengthening techniques to effectively control cracking. Additionally, examine the use of anchors with externally bonded fiber sheets to enhance bonding efficiency. The design of this approach aims to reduce the risk of premature debonding, prevent strengthening failure before rupture, and enhance the overall effectiveness of the strengthening process. A total of ten reinforced concrete two-way slabs were fabricated and subjected to progressive static loading for testing purposes. The examined slabs all have identical measurements: 100 mm for thickness, 1100 mm for width, and 1100 mm for span. All specimens were divided into two groups: Group I included two slabs, one of which was solid without openings, and the other had a central square opening measuring 300 mm. Group II consisted of eight slabs, all of which had a central square opening measuring 300 mm. In group I, the reference two-way slab without openings was not strengthened, nor was the reference two-way slab with a central opening strengthened. In group II, five two-way slabs were strengthened using externally bonded glass fiber-reinforced polymer (EB-GFRP) sheets on the tension side. One two-way slab was internally strengthened by using reinforcing steel bars around the opening. Additionally, two two-way slabs were strengthened using the near-surface-mounted technique (NSM). Specimens were loaded until failure occurred. Failure modes, cracking patterns, ultimate loads, and load-deflection relationships of all slabs were computed and contrasted for both groups, where the different strengthening techniques contributed to increasing the load capacity by 15–40 percent compared to the reference slab with an opening. In this study, experimental testing, theoretical equations, and finite element modeling using the ABAQUS program were used to evaluate the performance of RC two-way slabs with openings under various strengthening configurations. The results of the experimental tests, theoretical equations, and finite element modeling demonstrated a high degree of agreement, with the average ratio of theoretical to experimental ultimate load (P_{The}/P_{Exp}) ranging from 0.92 to 1.03, and the average ratio of finite element to experimental ultimate load (P_{FE}/P_{Exp}) ranging from 1.00 to 1.09.

1. Introduction

Occasionally, a building's structural needs necessitate the creation of apertures in pre-existing reinforced concrete slabs to accommodate various facility requirements, such as the installation of elevators, staircases, or utilities like air conditioning, sewage pipes, or electric ducts. Nevertheless, the act of making a cut-out in slabs results in a disruption of the slabs' continuous loading paths [1–5]. People often overlook the structural implications of small apertures because the structure can disperse pressure. However, when large openings require the extraction of substantial quantities of concrete and reinforcing steel, the static system may undergo modifications. Consequently, the diminished capacity of the structure to withstand the applied forces necessitates its strengthening. Despite taking all necessary measures, the process of creating openings in existing R.C. slabs remain a significant

* Corresponding author.
E-mail addresses: Mohamed.A.Ahmed@bhit.bu.edu.eg (M. AbdelBaset), mohamedmakhlouf83@yahoo.com (M.H. Makhlouf), marwa.hani@bhit.bu.edu.eg (M.H. Bondok), gamal.ismail@bhit.bu.edu.eg (G.I. Khaleel).

https://doi.org/10.1016/j.istruc.2025.108361
Received 21 August 2024; Received in revised form 7 January 2025; Accepted 1 February 2025

Nomenclatures

R.C	Reinforced concrete
NSM	Near surface-mounted
EB-GFRP	Externally bonded glass fiber-reinforced polymer
EB-CFRP	Externally bonded carbon fiber-reinforced polymer
LVDT	Linear variable displacement transducer
FEM	Finite element model
FEA	Finite element analysis
CDP	concrete damaged plasticity
P_{cr}	Cracking load
P_u	Ultimate load-carrying capacity
$P_{u,\ Exp.}$	Ultimate load-carrying capacity from Experimental
$P_{u,\ FE.}$	Ultimate load-carrying capacity from FEA
$P_{u,\ Th.}$	Ultimate load-carrying capacity from Theoretical
Δ_{cr}	deflection at cracking load
Δ_u	deflection at the ultimate load
D_I	Ductility index
K_i	Uncracked stiffness
K_u	Ultimate stiffness
Φ	Nominal diameter of reinforcing bar
E	Elastic modulus
E_s	Modulus of elasticity for steel reinforcement
A_s	Area of steel reinforcement
fs	Steel's tensile stress
d_s	Effective depth
β_1	Concrete stress block
C	Depth of neutral axis
f_f	Fiber's effective tensile stress
d_f	Effective depth for GFRP
A_f	Cross-section area for GFRP
Ψ_f	Reduction factor for the strength of FRP
ε_s	Steel tensile strain at failure
ε_{fe}	Effective tensile strain in FRP
ε_{bi}	Existing tensile strain at slab's bottom
f'c	Concrete's cylindrical compressive strength
$\acute{\varepsilon}_c$	Concrete's compressive strain at f'c
ε_c	Concrete's compressive strain at failure
σ_e	yield stress
ε_p	plastic strain at yield stress
υ	Poisson's ratio
σ	Normal stress
σ_c	Compressive stress of concrete
σ_t	Tensile stress of concrete
ε	Strain
ε_t	Tensile strain of concrete
ε_c	Strain of concrete
P_{add}	the additional load
δ	The deflection
M_{add}	the additional moment
T_{add}	the additional tensile force
d_{add}	the effective depth due to the increased strengthening
θ	the angle of rotation of rods passing through two segments of the slab

matter that requires examination [6]. These perforations frequently diminish the load-carrying capacity, stiffness, and deflection control of the slabs. Earlier studies commonly addressed the reduction in reinforcement due to openings in RC slabs by exclusively adding extra strengthening material to the tension side of the slab [1–3,5,7,8]. Nevertheless, it is crucial to acknowledge that the cut-out impacts both the reinforcing steel and the concrete. Reinforcing the tension steel during a cut-out in the concrete section increases the forces applied to the concrete on the compression side. This increase in forces might result in compression failure, particularly in sections that have a significant amount of reinforcement. Moreover, strengthening the tension steel alters the neutral axis position in the reinforced concrete section, reducing the resisting moment's arm. Consequently, the previous strength cannot be completely regained, and a substantial decrease in ductility is expected. The strengthening procedures generally succeeded in restoring the slab's flexural capacity [9]. Researchers have conducted several studies [1–5,8,10–14] to assess the impact of openings on slabs. The predominant focus of these studies has been to analyze the behavior of one-way R.C. slabs that already have openings [1–5,8,14–21], with a smaller number of studies examining the behavior of two-way R.C. slabs [10,22–29]. Studies by [4,30,31] revealed that larger openings (greater than 15 % of the slab area) resulted in up to a 50 % reduction in flexural capacity, whereas circular openings caused less severe stress concentrations compared to rectangular ones. [32] observed that openings near the slab's center amplified deflections and bending moments, while edge openings primarily affected shear capacity. An investigation was conducted on the methodology of strengthening, the composition of the materials employed, and the cost-effectiveness of the process. Researchers have developed various techniques to enhance the structural integrity of specific R.C. slabs. These procedures include section expansion, concrete repair, and external plate bonding utilizing either steel plates or fiber-reinforced polymer (FRP) plates or sheets. It is a typical practice to enhance the strength of reinforced concrete slabs by applying an additional layer of concrete [33]. Nevertheless, connecting a new layer of concrete to an existing concrete structure may lead to problems with long-term strength and stability, such as layer separation or crack formation at the point of connection. Temperature changes, shrinkage, or a combination of these factors can cause movement, leading to these concerns [34,35]. Hence, it is crucial to provide thorough surface preparation and employ suitable shear connectors to link the two layers [36]. Externally Bonded (EB) steel plates, affixed via either bolting or adhesive bonding, provide an alternative approach to enhancing the strength of structures. Studies have shown that EB steel plates are useful in improving a material's ability to bend without breaking and reducing the width of cracks and deformations under different degrees of load [37–39]. Nevertheless, these outer steel plates are vulnerable to corrosion, which requires additional expenses for safeguarding. Furthermore, using mechanical anchorage rather than epoxy adhesive may cause tension to accumulate at the anchorage zone [39]. On the other hand, fiber-reinforced polymer (FRP) materials have several benefits, such as high strength, low weight, and resistance to corrosion, which have resulted in their extensive use in recent times.

Numerous studies have examined the strengthening of reinforced concrete (R.C.) slabs with cutouts using the EB technique [8,40–42]. Researchers noted that the fiber-reinforced polymer FRP-strengthened slabs showed higher load-carrying capacities compared to the non-strengthened slabs. However, the majority of the FRP-strengthened slabs failed due to the FRP's separate from the concrete surface, which initiated cracks at the concentrated corners. The debonding mode referred to here is well recognized as intermediate crack-induced interfacial debonding, or simply intermediate crack debonding [7,8,40]. Researchers extensively used carbon fiber-reinforced polymer CFRP strips to strengthen RC slabs with cuts, enhancing their load-carrying ability and stiffness. Several studies [3,8,9,11,14,22,24,30,31,43–45] have supported this. Research has shown that using CFRP strengthening techniques can enhance the load-carrying capacity of the slab. Research has proven that the NSM CFRP technique is more successful than EB CFRP [43]. Furthermore, CFRP has proven advantageous in impeding the occurrence of cracks and diminishing their width [11,46]. Using anchors in conjunction with CFRP has effectively avoided debonding

Table 1
Details of the tested specimens.

Group	Specimen ID	Opening size (mm)	Strengthened Technique	Strengthening Configuration
I	SS	without	———	without strengthening
	SO	300 × 300	———	without strengthening
II	SO-G-1P	300 × 300	EBR	One layer of GFRP sheet partially covers the tension surface
	SO-G-2P	300 × 300	EBR	Two layers of GFRP sheets partially cover the tension surface
	SO-G-F	300 × 300	EBR	One layer of GFRP sheet fully covers the tension surface
	SO-G-1P.A	300 × 300	EBR	One layer of GFRP sheet with anchors partially covers the tension surface
	SO-G-1P.R	300 × 300	EBR	One layer of GFRP sheet, with GFRP rods in the corners, partially covers the tension surface
	SO−1GR	300 × 300	NSM	One GFRP rod along the edges, at the tension surface
	SO−1SR	300 × 300	Inner	One steel rod along the inner edges of the concrete
	SO-G-1P.L	300 × 300	NSM	One layer of GFRP sheet partially covers the tension surface with a layer of concrete

and allowed the CFRP strip to achieve its maximum tensile capacity [1, 32]. Nevertheless, it is crucial to acknowledge the many limitations of CFRP, including its substantially higher cost compared to conventional reinforcing steel bars and the fact that its structural performance is critically influenced by the accuracy of installation methods and the specific conditions of load application. [47] demonstrated that hybrid FRP sheets, combining carbon and glass fibers, improved ductility and delayed debonding failure compared to conventional CFRP. [48] applied UHPC overlays as part of an EBR system, achieving enhanced stiffness and improved crack resistance.

The near-surface mounted (NSM) approach is employed to mitigate debonding failure by inserting strengthening rods or strips and filling material into pre-cut grooves along the concrete cover. This method provides decreased exposure to severe conditions and exhibits higher bond efficiency in comparison to the externally bonded (EB) technique because of its larger contact area with the underlying concrete. Because of this, NSM is less likely to fail when debonding than EB with FRP strips [4,29,49] and is better at sticking to the FRP material. This makes it easier for the high tensile stress in the FRP material to be mobilized, which stops early debonding failure and improves the strengthened part's ability to hold weight [50,51]. Nevertheless, FRP materials still have several disadvantages, including limited fire resistance, which results in high fire protection expenses [52]. The integration of EBR and NSM methods has shown significant promise in maximizing the benefits of each technique. [53,54] combined CFRP sheets (EBR) with GFRP rods (NSM) for strengthening RC slabs with large openings. The results demonstrated a 75 % improvement in flexural capacity and better crack control compared to using either technique alone. Numerical simulations using Finite Element Analysis (FEA) have become integral to studying the behavior of R.C. slabs with openings. Researchers have conducted numerous studies using a non-linear finite element model (FEM) to investigate the behavior of two-way RC slabs. The concrete damaged plasticity (CDP) model is widely used to simulate concrete cracking and failure. The results of previous studies showed a strong correlation between the theoretical and experimental results [55–58], underscoring the dependability of the analytical methods.

1.1. Research significance

Despite advancements in structural design codes, there are still significant limitations in addressing the behavior of reinforced concrete slabs with openings. Current codes focus on standard slab designs and provide limited guidance for cases including openings, which disrupt load transfer and create stress concentrations. Many researchers have focused their studies on analyzing the flexural behavior of one-way R.C. slabs that already have openings, while a smaller number of studies have examined the flexural behavior of two-way R.C. slabs with an opening. Various materials and techniques have been employed for R.C. slab strengthening; however, the use of externally bonded fiber-reinforced sheets has exhibited notable limitations. These challenges primarily stem from premature debonding, which results in a failure of the strengthening system before the rupture stage is reached. This research aims to study the flexural behavior of two-way R.C. slabs with an opening, investigate the impact of using anchors with externally bonded fiber sheets to improve the bonding effectiveness, conduct detailed experimental tests, theoretical equations, and finite element modeling to assess the flexural performance of slabs with openings, and provide practical recommendations for optimizing strengthening strategies in structural applications. In this research, ten square two-way R.C. slabs with an opening were tested, which were strengthened using different techniques such as NSM, EBR, and INNER. Eventually, the test failure loads were compared to the predicted failure values obtained from the analytical values of the ACI 440–2R-17 equations [59]. Additionally, a non-linear finite element model (FEM) was conducted to verify the effectiveness of the tested slabs using ABAQUS software.

2. Experimental program

2.1. Study parameters

In this study, 10 two-way R.C. slabs were created and subjected to gradual increases in static load for testing purposes. All slabs that were tested have identical dimensions, with a thickness of 100 mm, a width of 1100 mm, and a span of 1100 mm. A carefully selected set of key variables was utilized in this study, including: introducing openings in the slabs to assess their impact on structural performance; using GFRP sheets to provide either full or partial surface coverage, and analyzing the effects of each approach; incorporating anchors with GFRP sheets to enhance bond strength and minimize debonding; applying a concrete layer above the GFRP sheets to improve overall performance and offer fire protection; varying the number of GFRP sheets to evaluate their influence; and employing both internal steel bars and near-surface mounted (NSM) GFRP rods to examine the effectiveness of different strengthening techniques. The parameters and slab codes are provided in Table 1. The code of each slab consists of several symbols. For example, the symbols (S, O) represent slabs with and without an opening, while (F, P) represent slabs with a full or partial GFRP sheet. The symbols (1 P, 2 P) indicate the number of partial GFRP layers; (1 P. A) represents a slab with one layer of GFRP with anchorage; (1 P. R) represents a slab with one layer of GFRP and a GFRP rod at the corner of the opening; (1 P. L) represents a slab with one layer of GFRP and a layer of concrete; and (GR, SR) represent a rod made of GFRP or steel.

2.2. Slab reinforcement details

The main reinforcement was comprised of 10 mm-diameter deformed steel bars. The bars were interconnected using wire to create a mesh with a uniform spacing of 215 mm in both horizontal and vertical directions, as depicted in Fig. 1(a, b). Table 2 displays the characteristics of steel reinforcement. A strain gauge was used from type FLAB-10–11–1LJC-F, a product made by Tokyo Measuring Instruments Lab; gauge length: 10 mm (length of the area over which strain is measured); gauge factor: 2.08 ± 1 % (sensitivity of the strain gauge);

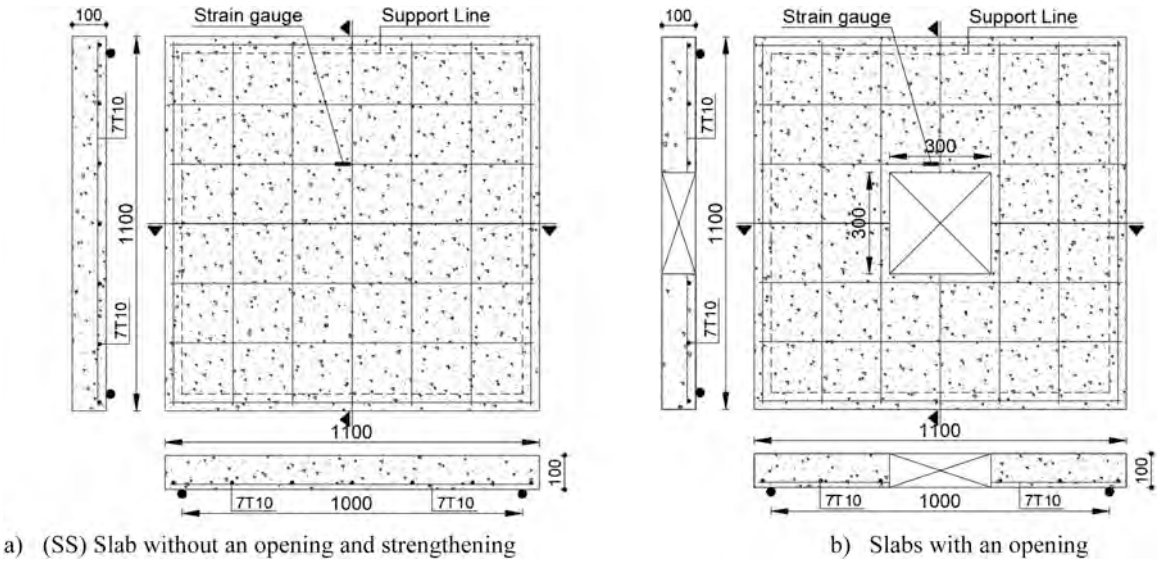

Fig. 1. Schematic of reinforcement details for all tested slabs (all dimensions in mm).

Table 2
Characteristics of steel reinforcement.

Size - mm	Cross-section area - mm^2	Yield strength - MPa	Ultimate strength - MPa
Φ10	78.5	570	785

Table 3
Mix components of concrete.

Components	Quantity
Cement - kg/m^3	323
W/C	0.62
Fine aggregate - kg/m^3	792
Coarse aggregate - kg/m^3	1056

gauge resistance: 120 Ω ± 0.5 Ω. A single strain gauge was affixed to the midpoint of the reinforcing bar adjacent to the opening in the X-direction for the tested slabs, as shown in Fig. 1(a, b). To prepare the reinforcing rebar for connection, the surface is made smooth by removing and cleaning the deformed ribs. Subsequently, a water-resistant tape is applied over the strain gauge to safeguard it during concrete placement and prevent any absorption of moisture.

2.3. Concrete mixture

The trial mixes were conducted at the reinforced concrete laboratory of the Benha Faculty of Engineering in this study. Table 3 provides a detailed list of the essential ingredients required for the preparation of the concrete mixture. To achieve a compressive strength of 25 MPa in reinforced concrete, ordinary portland cement (OPC) (42.5 N) was used, fine aggregate (sand) with a typical size ranging from 0.25 to 2.0 mm, and coarse aggregate (gravel) with a size ranging from 5 mm to 20 mm. After a period of 28 days, a suitable combination was chosen in order to get the targeted cubic compressive strength of 25 MPa. The concrete samples underwent compressive strength testing according to BS EN 12390–3, with a loading rate of 0.5 MPa/sec [60].

2.4. GFRP strengthening system

In this study, glass fiber polymers were used with the epoxy resin, which consists of two components A and B, where component (A) is the resin and component (B) is the hardener, as illustrated in Fig. 3. Glass fiber sheets were affixed to the tension surface of the slab. The sheets, with dimensions of 150 mm in width and 1000 mm in length, were positioned in both orientations along the perimeter of the opening. One specimen was strengthened using two layers of sheets, while the other specimens were strengthened using only one layer. In addition, the tension face of one slab was strengthened with glass fiber rods. These GFRP rods have a diameter of 10 mm and a length of 1000 mm. Fig. 2 shows the strengthening of all specimens. Tables 4–6 show the characteristics of GFRP sheets, bars, and epoxy resin.(Fig. 3)

2.5. Test specimens

As shown in Figs. 1 and 2, the experimental work program included a reference slab without openings and nine RC two-way slabs with openings. The interior reinforcement steel and overall dimensions of each specimen were identical. Each slab measured 1100 mm in width, 100 mm in thickness, and 85 mm in effective depth. Each slab's overall length was also 1100 mm. All slabs had an effective width of 960 mm. For this study, an opening size of 300 × 300 mm was examined. All openings were located in the area of the structure with the highest moment, and the length of the opening was aligned with the slab's transverse direction. Each specimen was strengthened using a solitary mesh composed of high-strength deformed steel rods (specifically, type B420DWR, according to the ECP-203 code [61]). The mesh utilized was comprised of 7 rods with a diameter of 10 mm in both directions. To simulate an opening in a manufactured slab, as depicted in Fig. 2, zero supplementary reinforcement was applied around the perimeter of the openings. The ten slabs were separated into two groups. The initial group (I) contained two slabs, one of them being solid (SS) and the other having a central square opening measuring 300 mm (SO), both of which were without any strengthening. Moreover, these slabs were utilized as reference points. The second group (II) consisted of eight slabs, each having a central square opening of 300 mm. Out of these, five slabs were strengthened with externally bonded glass fiber-reinforcing polymer (EB-GFRP) laminates on the tensile face. GFRP sheets measuring 1000 mm in length were used for strengthening. The first specimen labeled (SO-G-F) was strengthened with a single layer of GFRP measuring 350 mm in width, covering the entire tensile surface. The second and third specimens labeled (SO-G-1P) and (SO-G-2P) were strengthened with one and two layers of GFRP measuring 150 mm in width, respectively, around the opening. The fourth specimen labeled (SO-G-1P.A) was strengthened with a single layer of GFRP measuring

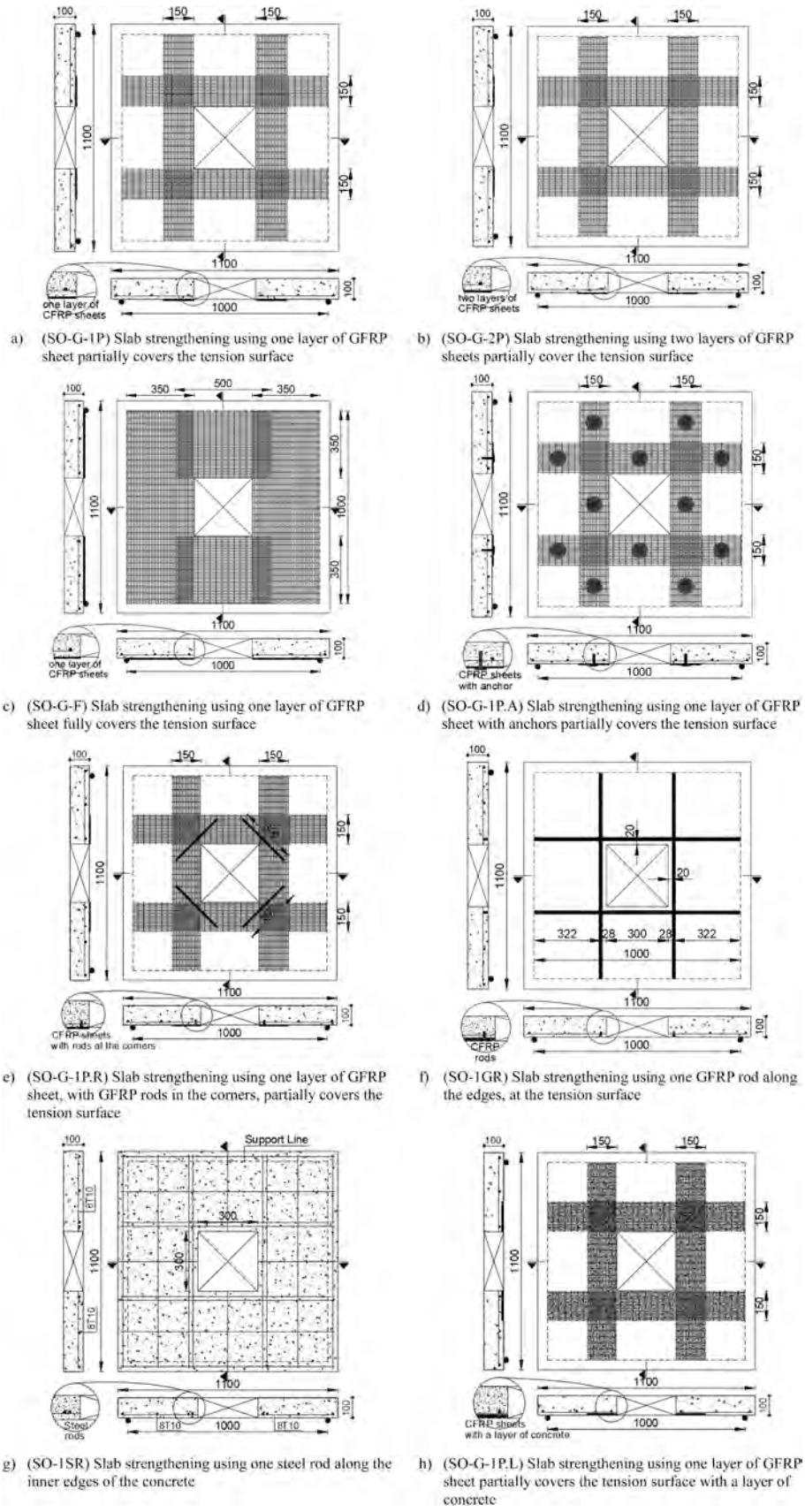

a) (SO-G-1P) Slab strengthening using one layer of GFRP sheet partially covers the tension surface

b) (SO-G-2P) Slab strengthening using two layers of GFRP sheets partially cover the tension surface

c) (SO-G-F) Slab strengthening using one layer of GFRP sheet fully covers the tension surface

d) (SO-G-1P.A) Slab strengthening using one layer of GFRP sheet with anchors partially covers the tension surface

e) (SO-G-1P.R) Slab strengthening using one layer of GFRP sheet, with GFRP rods in the corners, partially covers the tension surface

f) (SO-1GR) Slab strengthening using one GFRP rod along the edges, at the tension surface

g) (SO-1SR) Slab strengthening using one steel rod along the inner edges of the concrete

h) (SO-G-1P.L) Slab strengthening using one layer of GFRP sheet partially covers the tension surface with a layer of concrete

Fig. 2. Schematic figure for the details of strengthening of slabs (all dimensions in mm).

Table 4
Mechanical properties of GFRP sheets.

Property	SikaWrap® - 430 G
Fibre type	E-glass fibres
Laminate tensile strength - MPa	1500
Thickness - mm	0.168
Elastic modulus – Mpa	70000
Area density	430 g/m2 + 10 g/m2 (glass fibres only)
Dry fiber elongation at break	2.7 %

Table 5
Mechanical properties of GFRP bars.

characteristic	Glass-FRP-bars
Size - mm	10
Nominal area - mm^2	78.5
Tensile stress - MPa	1320
Elasticity modulus (E) - MPa	50000
Elongation at rupture - %	2.20

Table 6
Adhesive's characteristics.

Property	Amount
Compressive strength - MPa	110
resins strength on reinforcement – MPa	26
resins strength on RC - MPa	2 (concrete failure)
Modulus of elasticity - MPa	12800

150 mm in width, and a GFRP rod was used for anchorage. Lastly, the fifth specimen labeled (SO-G-1P.R) was strengthened with a single layer of GFRP measuring 150 mm in width and a GFRP rod measuring 10 mm in diameter and 300 mm in length placed at the corner of the opening. Two slabs in this group were strengthened using the Near Surface Mounted (NSM) technique on the tensile face. The sixth sample (SO-G-1P.L.) was strengthened by adding a single layer of GFRP that was 150 mm wide and 1000 mm long, together with a layer of concrete cover. On the other hand, the seventh sample (SO-1GR) was strengthened by adding a single rod of GFRP that was 10 mm in diameter and 1000 mm long on either side of the opening. The internal strength of the eighth sample (SO-1SR) was strengthened by adding a reinforcing steel bar on each side of the opening. Fig. 4 shows the preparation of strengthening techniques.

2.6. Test setup

The laboratory uses the heavy steel frames that constitute the test setup. The loading system consists of a set of interconnected frames with high reaction strength, attached to a hydraulic jack with a force capacity of 1000 kN. This jack operates using an electric pump with an equivalent load capacity. A load cell was placed beneath the hydraulic jack to measure the applied force. Test data were recorded and stored on a computer using a data collection system. In this study, all samples were simply supported on all four sides and placed on a set of interconnected steel sections forming a 1000 × 1000 mm square to simulate the presence of beams in real conditions. These sections were steel boxes with dimensions of 100 × 100 x 5 mm, and load was applied at four points. The loading configurations for the slabs with an opening are shown in Fig. 6a, where loads were applied at quarter spans along each side. The vertical load was transferred through a main rigid beam of steel I-beam, then to two parallel beams of steel I-beam, then to four concrete cubes with dimensions 150 mm, and finally to the loaded areas on the surface of the tested slabs. This setup applied a central vertical load to four specific points on the slabs' top surfaces, as illustrated in Fig. 5. To observe the behavior of the specimens being tested, a slow and controlled loading rate of 0.02 millimeters per second was implemented. To monitor vertical deflection, four LVDTs were positioned on the underside of the specimens, aligned with the concentrated load points. The LVDTs were installed on independent frames isolated from the slab and supports to ensure precise measurements of vertical displacement. These frames were fixed securely to prevent movement or vibrations during testing to ensure the elimination of any potential data loss or inaccuracies. Fig. 6b shows the location of the LVDT. Cracks visibly extended until the slabs ultimately failed.

2.6.1. Test setup limitations

The experimental test setup had specific limitations, including the loading frame capacity of 1000 kN, which constrained the applied loads to scaled-down specimens. The supports were modeled as rigid, replicating idealized boundary conditions, which may differ from real-life scenarios. Measurements from LVDTs and strain gauges were highly precise but subject to minor placement sensitivities. Additionally, all tests were conducted under controlled laboratory conditions, excluding environmental factors like temperature or humidity. These limitations were considered in the analysis, and future studies are recommended to address them through larger-scale and real-life testing.

3. Experimental results of slabs

The test results of groups I and II were compared to assess the efficacy of the strengthening techniques. The main objective was to verify the efficacy of the strengthening technique in enhancing the load-bearing capacity of the slab and controlling deflection. In general, certain specimens exhibited a greater load-carrying capability compared to the reference specimens. Table 7 shows a brief summary of the test outcomes.

3.1. Cracks patterns and mode of failure

Fig. 7 illustrates the crack patterns and collapse in all tested specimens, for reference specimens of two-way R.C. slabs, denoted as SS and SO, with and without an opening, respectively. Cracks were primarily found on the lower tension surface of the reference slab (SS). The main cracks exhibited a parallel alignment with the slab's diagonals. It was observed that narrower cracks were running parallel to the initial cracks throughout the slab. Conversely, in the case of the slab with an opening (SO), cracks initiated at the corner of the opening and propagated toward the edges of the slab, persisting until the point of failure. Both slabs collapsed, mainly due to flexural and punching shear failures. Comparing the crack patterns on both slabs revealed that the opening's presence significantly increased the number of cracks.

For slabs SO-G-1P, SO-G-2P, SO-G-1P.A., and SO-G-1P.R. These slabs

Fig. 3. Materials used for strengthening in this study.

Slab strengthening by EBR technique without anchors.

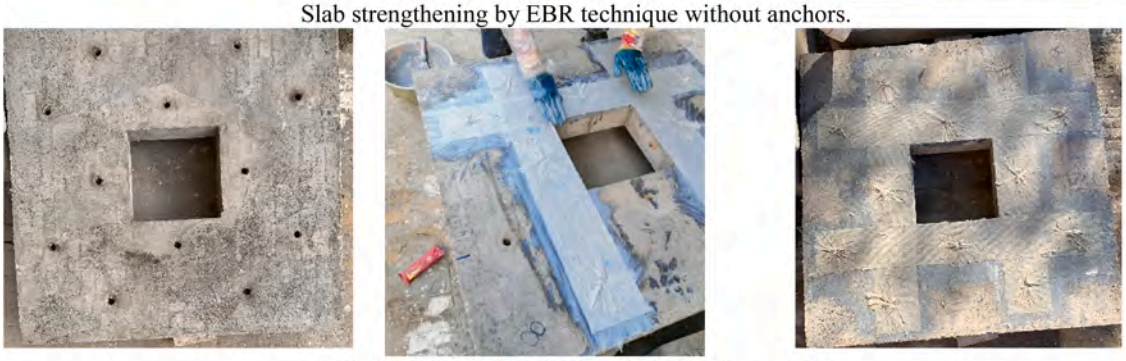

Slab strengthening by EBR technique with anchors.

Slab strengthening by EBR technique with rods at the corners of the opening.

Slab strengthening by NSM technique by adding a layer of concrete.

Slab strengthening by NSM technique with a GFRP rod along the edges of the opening.

Fig. 4. Preparation of various strengthening techniques.

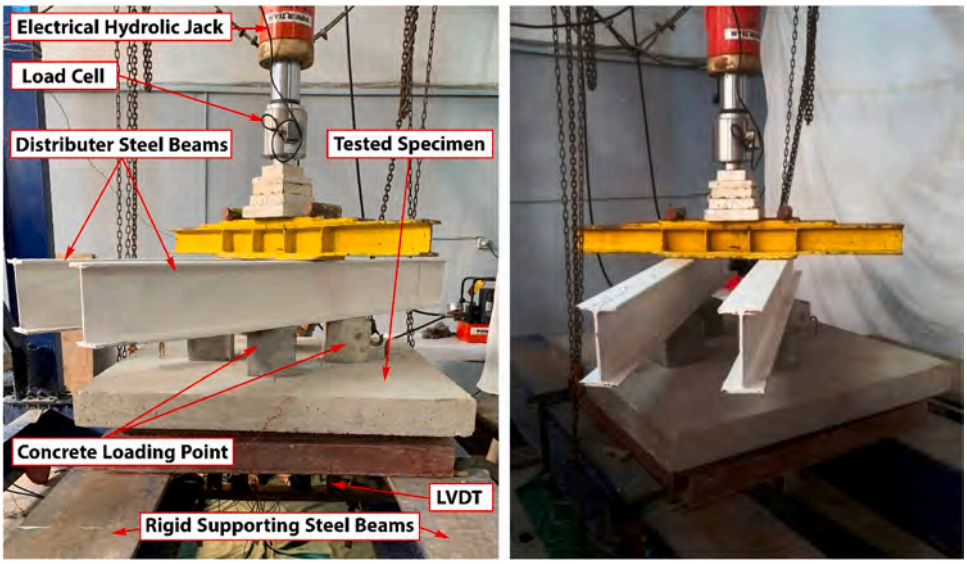

Fig. 5. Test setup.

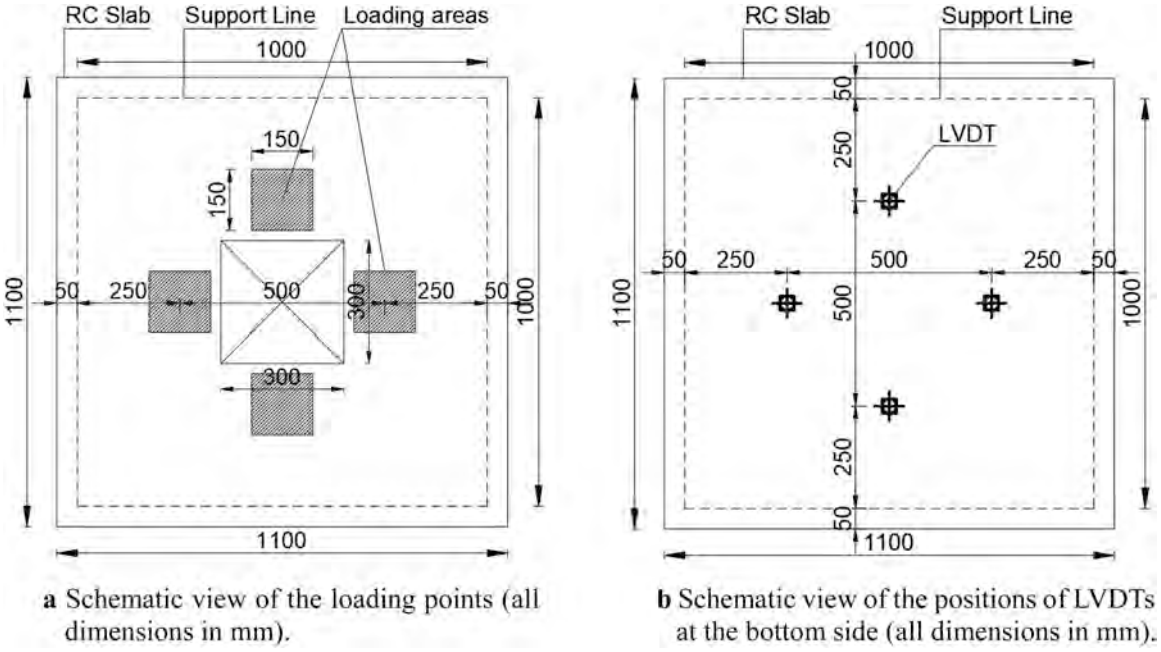

Fig. 6. a Schematic view of the loading points (all dimensions in mm). b Schematic view of the positions of LVDTs at the bottom side (all dimensions in mm).

were strengthened using several methods: one or two layers of GFRP, one layer of GFRP with GFRP anchors, and one layer of GFRP with GFRP rods positioned at the corners of the opening. Slabs SO-G-1P, SO-G-2P, and SO-G-1P.R. failed due to GFRP delamination and flexural mode, while the slab SO-G-1P.A. collapsed due to punching shear and flexural mode, as shown in Fig. 8. After analyzing crack patterns and failure loads, it was found that utilizing EB GFRP for strengthening the openings, particularly without anchors, is not recommended. The use of anchors may result in the slabs' behavior being variable, as seen in slab SO-G-1P.A. Weak adhesion between the GFRP layer and concrete, possibly due to the opening process, may have caused the failure in slabs SO-G-1P, SO-G-2P, and SO-G-1P.R.

For slabs, SO-1GR and SO-1SR were strengthened with GFRP bars using the NSM technique, and steel bars were inserted into the specimen before casting, specifically around the opening. Both slabs experienced failure due to punched shear and flexural modes. The placement of GFRP bars along the edge of the opening in SO-1GR effectively controlled crack patterns, preventing them from initiating from the corners. Conversely, in SO-1SR, the crack patterns were identical to those observed in SO, the control-tested slab. However, there was an increase in diagonal cracks due to the location of the concentrated load. The relationship between the number of cracks and the additional steel reinforcement around the opening was obvious, as increasing the maximum load led to an increase in the cracks.

A single layer of glass fiber-reinforced polymer GFRP sheet was used to strengthen all the tensile surfaces in slab SO-G-F. The complete coverage of the strengthening material concealed the crack patterns on the tension face. The slab failed due to the rupture of the GFRP sheets and punching shear modes, as shown in Fig. 8.

The slab SO-G-1P.L. was strengthened using the NSM technique, which involved adding a layer of GFRP sheets and an additional layer of concrete on top of it. Crack patterns developed from the corners and

Table 7
Summary of test results.

Specimen ID	P_{cr} kN	Δ_{cr} mm	P_{ul} kN	Δ_{ul} mm	$P_{ul}/P_{ul\ control}$ (SS) %	$P_{ul}/P_{ul\ control}$ (SO) %	DI Δ_{ul}/Δ_{cr}	Ki kN/mm	Ku kN/mm	Mode of failure
SS	75	2.72	320	18	1.00	1.36	6.62	27.57	16.03	I
SO	55	3.5	235	13.5	0.73	1.00	3.86	15.71	18.00	II
SO-G-F	90	3.95	329	17.73	1.03	1.40	4.49	22.78	17.34	IV
SO-G-1P	80	3	314	17	0.98	1.34	5.67	26.67	16.71	III
SO-G-2P	82	3.42	323	17.58	1.01	1.37	5.14	23.98	17.02	III
SO-G-1P.A	95	3.48	330	17.6	1.03	1.40	5.06	27.30	16.64	I
SO-G-1P.R	84	3.3	322	17.28	1.01	1.37	5.24	25.45	17.02	III
SO-G-1P.L	63	2.4	295	16.77	0.92	1.26	6.99	26.25	16.14	V
SO−1GR	80	3.52	280	16.2	0.88	1.19	4.60	22.73	15.77	I
SO−1SR	72	2.45	270	15.3	0.84	1.15	6.24	29.39	15.41	I

Note: P_{cr} = cracking load, Δ_{cr} = deflection at cracking load, P_{ul} = ultimate load, Δ_{ul} = deflection at ultimate load, DI = ductility index, Ki = uncracked stiffness, $Ki = \frac{P_{cr}}{\Delta_{cr}}$, Ku = ultimate stiffness, $Ku = \frac{P_{ul} - P_{cr}}{\Delta_{ul} - \Delta_{cr}}$, I = flexural and punching shear, II = flexural, III = punching shear, flexural, and GFRP debonding, IV = punching shear and GFRP rupture, V = punching shear, flexural and separating layer.

edges of the opening and extended towards the edges of the slab, matching the crack patterns observed in control slab SO. The failure mode was mostly caused by the separation between the additional layer and the concrete, as well as punching shear modes, as shown in Fig. 8.

3.2. Load-deflection relationship

Table 7 displays the initial cracking and ultimate loads for all tested slabs. Using several techniques for strengthening slabs with an opening result in a significant enhancement of both strength and stiffness. The strengthened samples showed higher ultimate loads and reduced deflection under equal loads compared to the reference slab with an opening. For all the tested slabs, Fig. 9 illustrates the relationship between the load and the deflection.

3.2.1. Effect of an opening

The effect of an opening on a slab (SO) is more noticeable when compared to a solid slab (SS) with the same size and concrete mixture, as depicted in Figs. 9a, 10, and 11. The solid slab SS exhibits a 36 % increase in ultimate load capacity in comparison to the slab with an opening, accompanied by a 24 % decrease in deflection under the same loading conditions. The difference in load capacity and deflection percentages can be explained by the fact that the concrete under the neutral axis, which has a larger cross-sectional area, helps to resist tensile stresses. In contrast, the slab with an opening has a smaller cross-sectional area under the neutral axis. A comparison of the results with previous studies [4,13,26,28,31] shows a clear agreement and consistency between the experimental results and findings in previous research.

3.2.2. Effect of the number of GFRP layers

The utilization of GFRP sheets to strengthen slabs, whether with one or two layers positioned at the tension surface of concrete slabs, has a positive impact on reducing deflection during both the cracking and ultimate stages. When comparing the effects of one layer of GFRP sheet on the strengthened specimen (SO-G-1P) to the un-strengthened specimen (SO), it was noticed there was a 34 % increase in ultimate capacity. At the same time, Fig. 9b shows a 22 % reduction in deflection. In contrast, the slab (SO-G-2P) strengthened with two layers of GFRP sheets exhibited a 37 % increase in ultimate capacity and a 41 % reduction in deflection compared to the specimen (SO), as depicted in Figs. 9b, 10, and 11. Comparing the effect of using one or two layers of GFRP sheet with strengthened specimens shows that slab (SO-G-2P) has a 2 % higher ultimate capacity and 7.5 % less deflection than slab (SO-G-1P). The stiffness of the slabs increases with the addition of more GFRP layers, aligning with a similar observation made by Soltani [62]. The number of GFRP sheets used, positioned around the opening at the tension face of the slabs, directly enhances the ultimate load capacity and reduces deflection. This setup helps prevent or minimize crack propagation by leveraging the high elongation properties of GFRP sheets.

3.2.3. Effect of strengthening technique

Using the EBR and NSM techniques to strengthen reinforced concrete slabs at the tension face has a positive impact on deflection and load capacity during the cracking and ultimate stages. The maximum loads and corresponding deflections of the tested specimens were compared, considering the impact of the opening and the applied strengthening technique. Slab (SO-G-1P), which was strengthened with GFRP sheets using the EBR technique, exhibits a 34 % increase in ultimate load capacity and a 22 % reduction in deflection compared to the without-strengthened specimen (SO). In contrast, the slab (SO-1GR), which was strengthened with GFRP rods using the NSM technique around the opening, exhibits a 19 % increase in ultimate load capacity and a 25 % reduction in deflection compared to the specimen (SO), as shown in Figs. 9c, 10, and 11. Comparing the failure loads of the same specimens with those of the reference specimen without an opening (SS), they were equal to 0.98 and 0.88, respectively. These results indicate that the EBR outperformed the NSM technique in terms of ultimate load capacity, although it did not surpass it in deflection. This is because the area of GFRP in sheets is not equivalent to the area of GFRP in rods.

3.2.4. Effect of strengthening configuration

The effect of the strengthening configuration was evaluated by comparing the performance of specimens SO-G-1P, SO-G-1P.A, and SO-G-1P.R. Each specimen was strengthened with a single layer of GFRP, incorporating anchoring and GFRP rods at the corners. The results showed a significant improvement in ultimate load capacity: 34 %, 40 %, and 37 % for SO-G-1P, SO-G-1P.A, and SO-G-1P.R, respectively. Additionally, there was a corresponding reduction in deflection by 22 %, 41 %, and 30 % compared to the slab with an opening (SO), as illustrated in Figs. 9d, 10, and 11. When compared to the ultimate load capacity of the control slab without an opening (SS), the ratios for the strengthened slabs were 0.98, 1.03, and 1.01, respectively. These findings highlight that the most effective strengthening method involved using a single layer of GFRP with anchorage. This configuration enhanced the bond between the GFRP sheets and the concrete by securing the sheets with GFRP rods, which included strands at their ends. The results suggest that combining the use of corner rods with anchors for fiber sheets can offer superior crack control and significantly improve load capacity. This dual-strengthening approach demonstrates the potential for achieving greater structural performance.

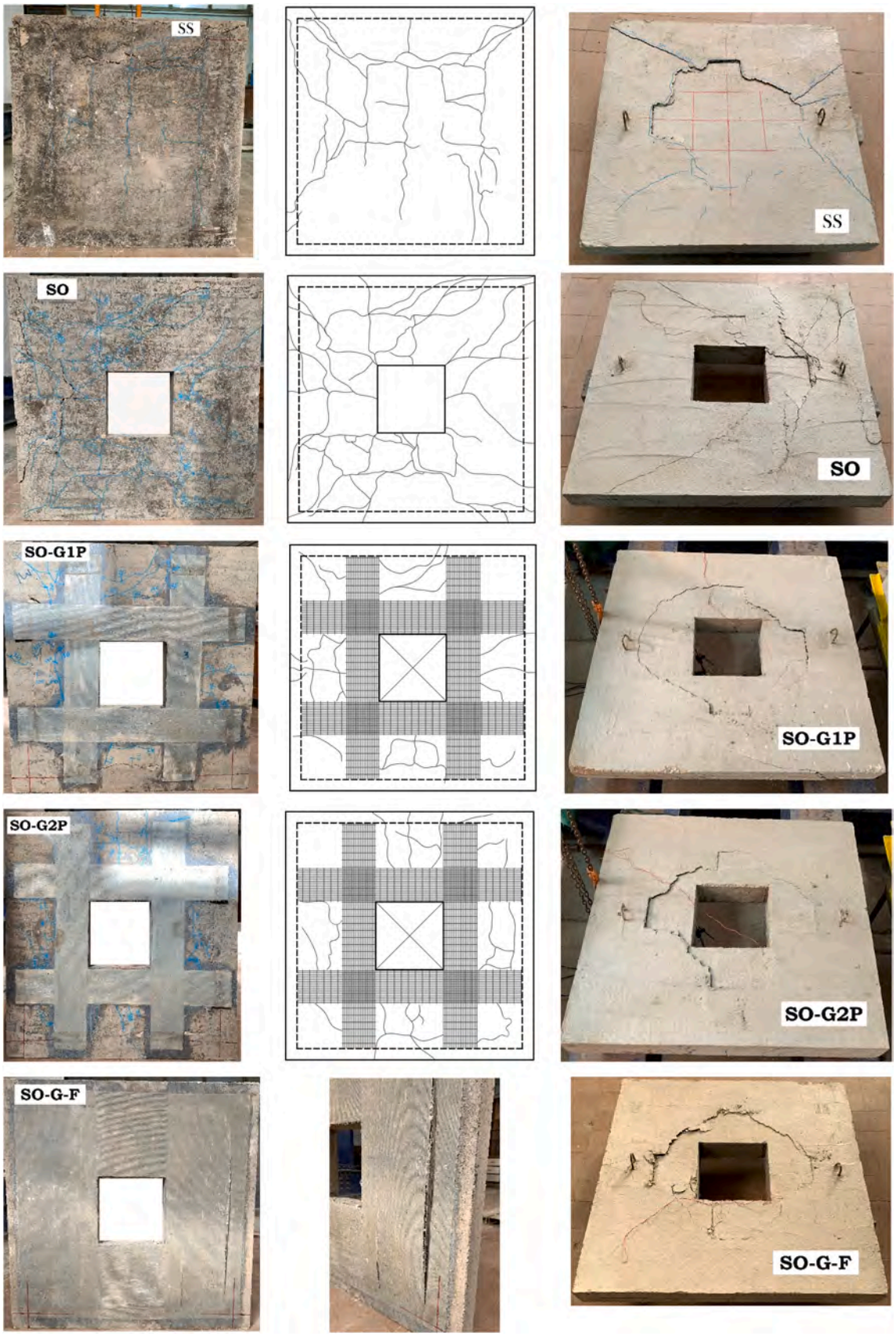

Fig. 7. Crack patterns at the bottom and top surface of all tested specimens.

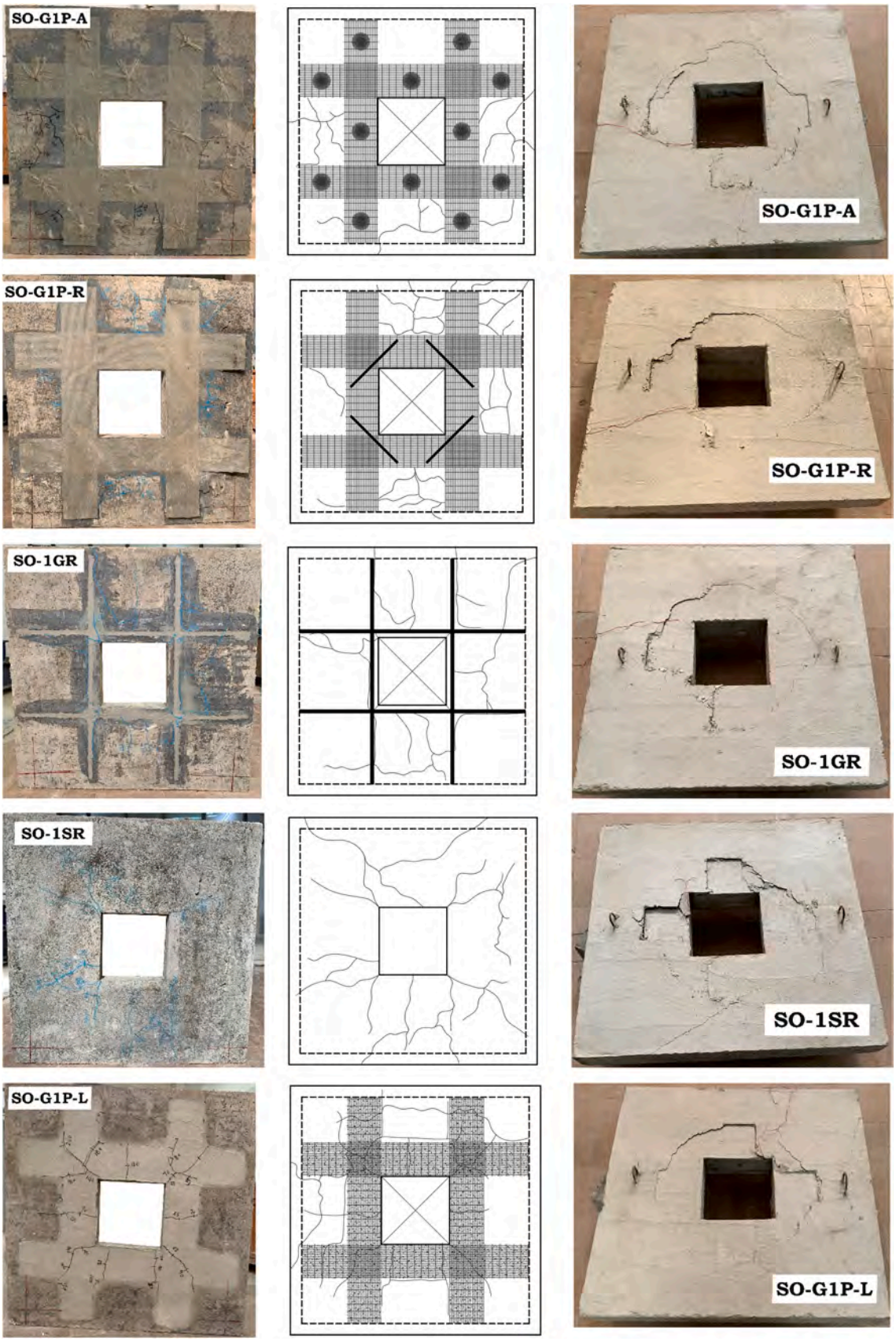

Fig. 7. (*continued*).

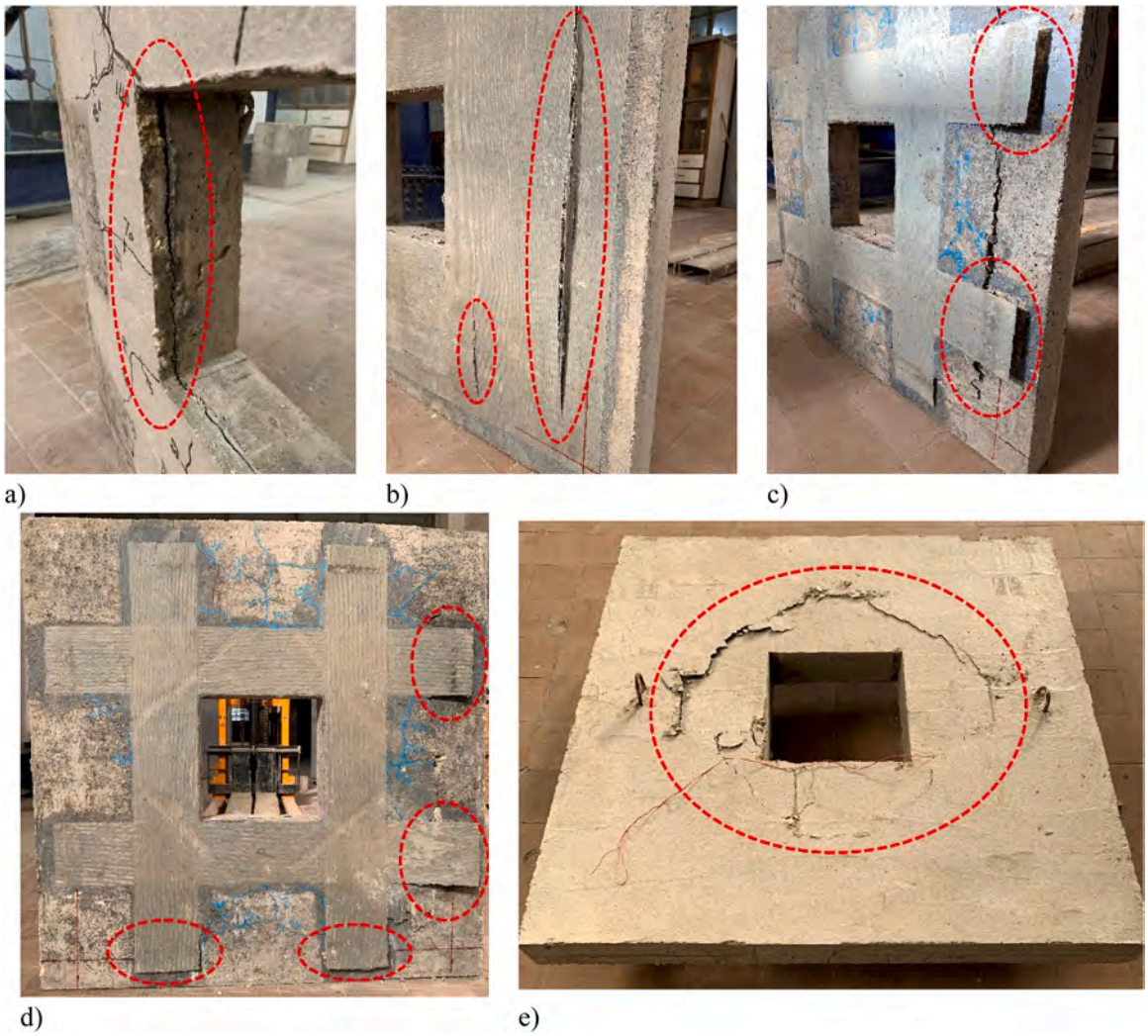

Fig. 8. Close-up shapes for modes of failure: a) separation between the additional layer and the concrete surface; b) rupture of the GFRP sheets; c and d) debonding between the GFRP sheets and the concrete; e) punching shear.

3.2.5. *Effect of adding a layer of concrete*

Although the EBR technique improves slab performance, it doesn't protect fiber sheets from high temperatures or fire. As a result, the effectiveness of adding a layer of concrete on top of the sheets was examined for added protection. The effect of adding a layer of concrete above the GFRP sheets can be evaluated by comparing the results of slabs SO-G-1P and SO-G-1P.L with reference slabs SS and SO. The last section referred to strengthening Slab SO-G-1P, while Figs. 2h and 4 illustrate the strengthening of Slab SO-G-1P.L with one layer of GFRP sheets and a layer of concrete. Slabs SO-G-1P and SO-G-1P.L exhibited a 34 % and 26 % increase in ultimate load capacity and a 22 % reduction in deflection for the two specimens compared to the slab without strengthening SO, as shown in Figs. 9e, 10, and 11. When comparing the ultimate load capacity of these slabs with that of the reference slab without an opening SS, they were found to be equal to 0.98 and 0.92, respectively. These results indicate that adding a layer of concrete on top of the fiber sheets results in a slight improvement compared to the sample strengthened with a layer of fiber without adding a layer of concrete. This is due to the separation that occurred between the added layer and the concrete, as shown in Fig. 8. The results of this method can be improved by adding dowels or anchorage to the concrete layer for bonding.

3.2.6. *Effect of full coverage for tension side*

The impact of complete coverage can be assessed by examining the outcomes of specimens SO-G-1P and SO-G-F. Specimen SO-G-F was strengthened with one GFRP sheet covering the entire tensile surface, while specimen SO-G-1P had one GFRP sheet covering the partially tensile face, as illustrated in Figs. 2a, c, and 4. The area covered by GFRP in the specimen SO-G-1P was 51 % of the area covered by GFRP in the specimen SO-G-F. As shown in Figs. 9f, 10, and 11, specimens SO-G-F and SO-G-1P exhibit a 40 % and 34 % increase in load capacity, with a 27 % and 22 % decrease in deflection compared to the un-strengthened slab SO, respectively. When comparing the maximum load capacity of these slabs to the reference slab without an opening SS, they were found to be 1.03 and 0.98, respectively. From these results, it is clear that full coverage of the slab on the tension side led to a relatively acceptable increase in the ultimate load capacity by 17 % and a decrease in deflection by 22 % compared to the same partially strengthened specimen. However, the drawback of this method is that cracks did not appear on the tension side due to the full coverage of the slab.

3.3. *Flexural stiffness of slabs*

Bending stiffness is defined as the ability of a structural element to withstand bending deformation. It is determined by various elements, including the elastic modulus, moment of inertia, effective length of the

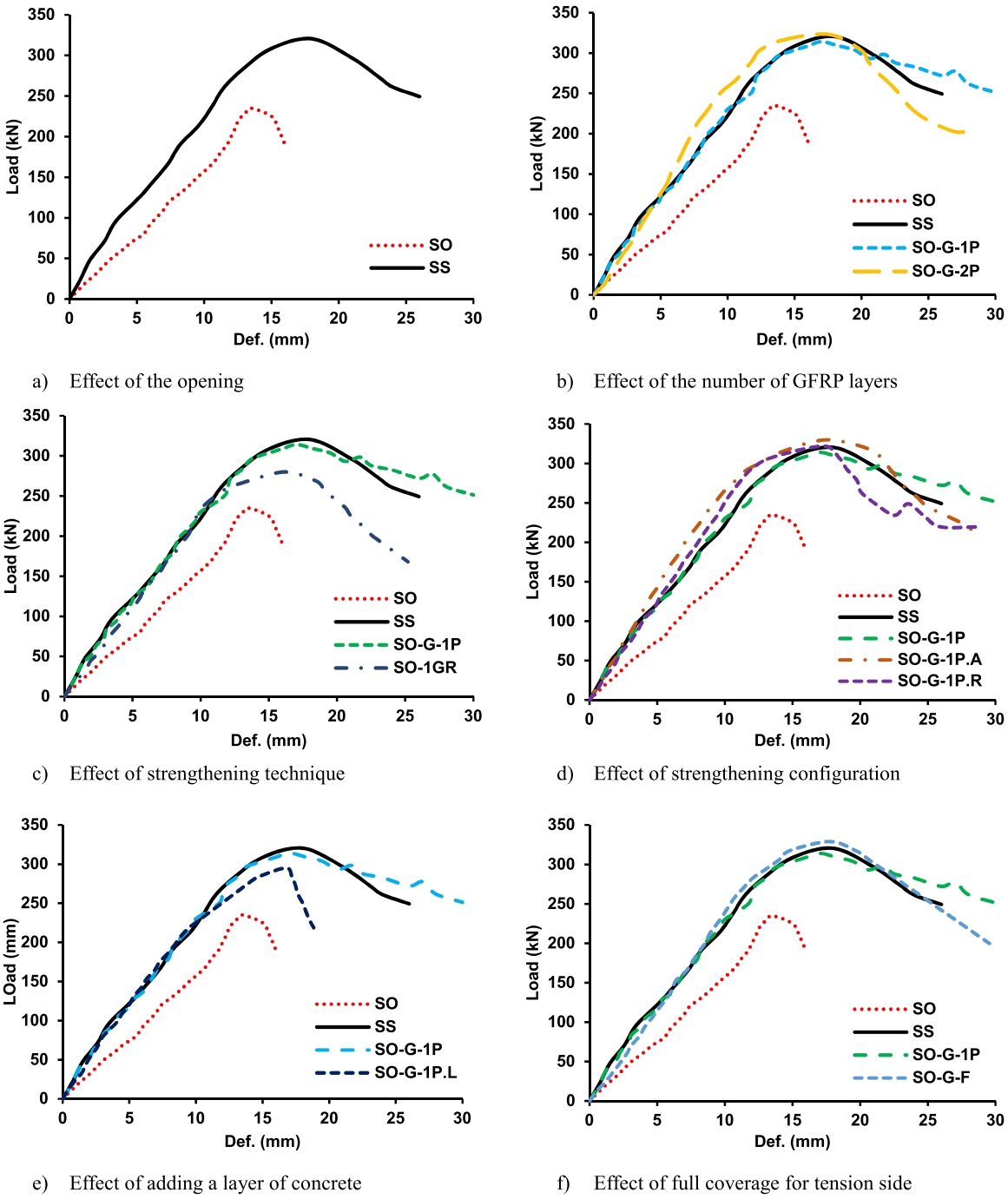

a) Effect of the opening

b) Effect of the number of GFRP layers

c) Effect of strengthening technique

d) Effect of strengthening configuration

e) Effect of adding a layer of concrete

f) Effect of full coverage for tension side

Fig. 9. Load deflection curves of all tested specimens.

element, and boundary conditions [63]. The secant stiffness was calculated using Eqs. (1) and (2). The stiffness values (K) for cracking and the ultimate stages are presented in Table 7. The stiffness exhibited a steady reduction during the loading process, with all ultimate stiffness values (Ku) being lower than the cracking stiffness values (Ki), as depicted in Fig. 12. This is likely attributed to the loading process inducing cracks and reducing the bonding between the concrete and steel bars. Utilizing GFRP sheets with anchors led to enhanced stiffness during both the cracking and ultimate loading stages. The greater stiffness-to-weight ratio of GFRP is responsible for enhancing the flexural rigidity of the specimens. The inclusion of GFRP layers resulted in an increase in the rigidity of the slab, which aligns with the conclusions drawn by Soltani [62].

$$K_i = \frac{P_{cr}}{\Delta_{cr}} \tag{1}$$

$$K_u = \frac{P_u}{\Delta_u} \tag{2}$$

3.4. Ductility of Slabs

Ductility is an important characteristic of reinforced concrete structures, as it enables the redistribution of forces and serves as a warning before failure. The inclusion of this characteristic is seen as essential in structural design codes because of its capacity to prevent abrupt and uncontrolled collapses. Ductile materials possess the ability

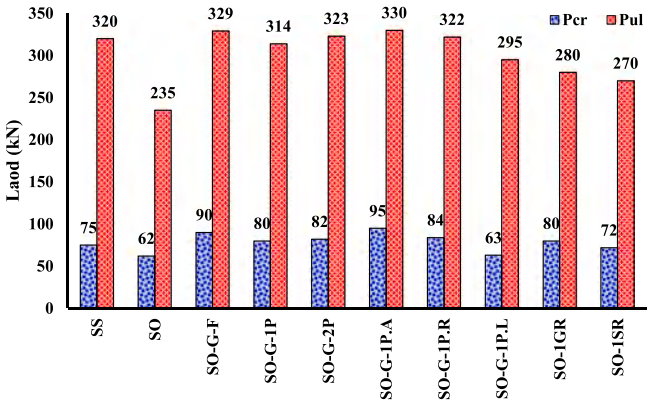

Fig. 10. Crack and ultimate load for all tested specimens.

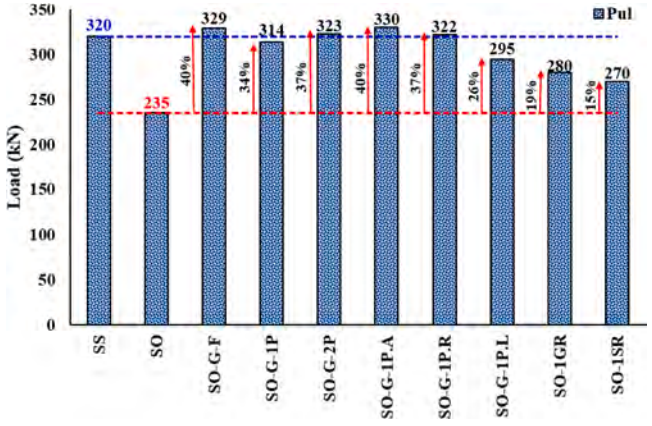

Fig. 11. Effect of an opening and different strengthening methods on ultimate load.

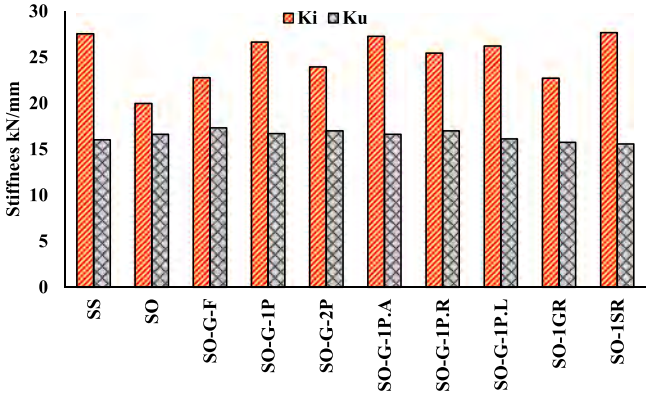

Fig. 12. Cracking and ultimate stiffness for all tested specimens.

to assimilate a substantial quantity of energy before breaking, in contrast to brittle materials, which can only assimilate a limited amount. The examination of ductility is conducted using a ratio called the ductility index (DI). The ductility factor was calculated by comparing the maximum displacement at the ultimate load (Δ_u) with the maximum displacement at the initial cracking load (Δ_{cr}). According to the data presented in Table 7, the slab that was strengthened with one layer of GFRP sheets and a layer of concrete showed better ductility compared to other samples. The addition of a layer to the concrete surface resulted in a significant increase in ductility, with an 81 % improvement compared to the reference slab (SO) with an opening, as shown in Fig. 13. This

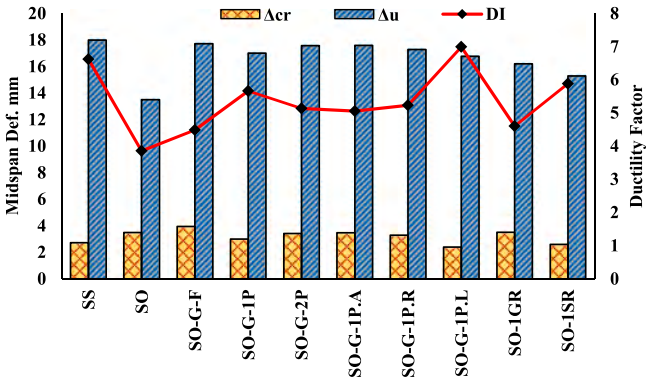

Fig. 13. Ductility index for all tested specimens.

improvement can be attributed to the early appearance of cracks caused by the separation between the new layer and the concrete surface. Sample SO-G-F, which had one GFRP sheet covering the entire tensile surface, showed a lower ductility index of 16 % compared to the reference slab (SO). This was mainly because it was difficult to detect cracks on the surface due to the complete coverage. Furthermore, the remaining samples showed comparable qualities of ductility.

4. Theoretical analysis

4.1. Theoretical analysis using ACI 440–2R-17

The analytical capacity values of all specimens, both with and without strengthening using FRP, were calculated based on the limiting condition rules. These rules require that internal force equilibrium and strain integration be satisfied at every cross-section. Additionally, the design conditions for the examined slabs were established. Based on the assumption that FRP would exhibit a stress-strain curve that is linearly elastic until failure and that there would be no sliding between the fiber and concrete, NSM bars or EB sheets were utilized as additional reinforcement with different material properties. The capacity of the tested slabs was determined using ACI 440–2R-17 [59] and then compared to the maximum load obtained by the testing data. The equations utilized are listed below:

$$M_{total} = \left[A_s f_s \left(d_s - \frac{\beta_1 C}{2}\right)\right] + \Psi_f \left[A_f f_f \left(d_f - \frac{\beta_1 C}{2}\right)\right] \quad (3)$$

Where A_s = area of steel reinforcement; f_s = steel's tensile stress at failure and can be calculated from Eq. (4); d_s = effective depth for steel reinforcement; β_1= concrete stress block factor; C = depth of neutral axis; f_f, d_f, A_f = effective tensile stress, effective depth, and cross-sectional area for GFRP, respectively. Ψ_f is reduction factor for the strength contribution of FRP reinforcement = 0.85.

$$f_s = E_s \quad \varepsilon_s \le f_y \quad (4)$$

Where ε_s = steel tensile strain at failure which can be calculated from Eq. (5), and E_s = modulus of elasticity for steel reinforcement.

$$\varepsilon_s = (\varepsilon_{fe} + \varepsilon_{bi})\left(\frac{d - c}{d_f - c}\right) \quad (5)$$

Where ε_{fe} effective tensile strain in FRP and can be calculated from Eq. (6); ε_{bi}= existing tensile strain at slab's bottom in case loading is present prior to strengthening [ε_{bi} = 0 in this study]. C, α_1, and β_1 can be determined from Eqs. (7–9).

$$\varepsilon_{fe} = 0.003 \quad \left(\frac{d_b - c}{c}\right) - \varepsilon_{bi} \quad (6)$$

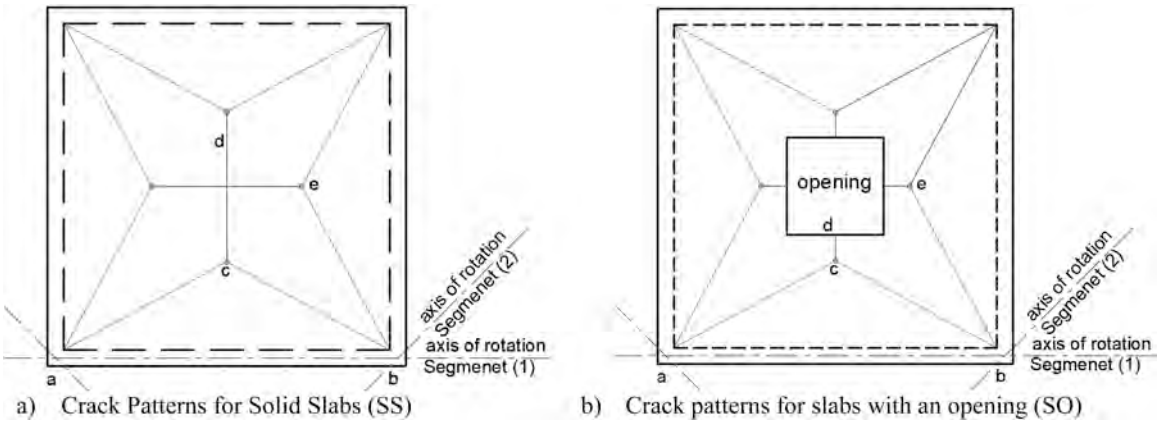

Fig. 14. Suggested crack patterns for the tested two-way RC control slabs (SS) and (SO).

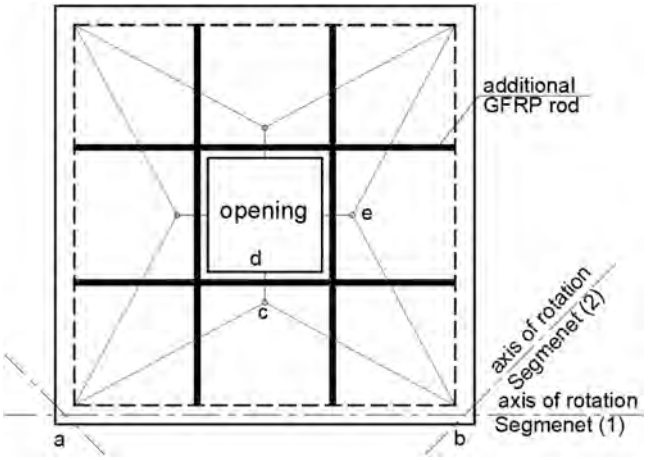

Fig. 15. Suggested crack patterns for the tested strengthened two-way RC control slabs.

$$C = \frac{A_s \ f_s + A_f \ f_b}{\alpha_1 \ f_c' \ \beta_1 \ b} \tag{7}$$

$$\alpha_1 = \frac{3 \ \varepsilon_c' \ \varepsilon_c - \varepsilon_c^{\ 2}}{3 \ \beta_1 \ \varepsilon_c'^{\ 2}} \tag{8}$$

$$\beta_1 = \frac{4\varepsilon_c' - \varepsilon_c}{6 \ \varepsilon_c' - 2 \ \varepsilon_c} \tag{9}$$

Where ε'_c = concrete's compressive strain at f'_c and can be found from Eq. (10) according to ACI-318 [64]; and ε_c = concrete's compressive strain at failure, determined from Eq. (11).

$$\varepsilon_c' = \frac{1.7 \ f_c'}{E_c} \tag{10}$$

$$\varepsilon_c = (\varepsilon_{fe} + \varepsilon_{bi})\left(\frac{c}{d_b - c}\right) \tag{11}$$

Table 10 and Fig. 22 show a comparison of the experimental data with the theoretical values for the ultimate load.

4.2. Theoretical analysis using Yield Line

Yield Line Design is a well-established approach for designing R.C. slabs and similar structural elements. It is based on yield line theory, which examines failure mechanisms at the ultimate limit state. The core principle of the theory is that external work equals internal work.

4.2.1. Energy dissipation

The experimental crack patterns observed in the slabs were used to propose yield line patterns for RC two-way slabs (SS) and (SO) with a central opening, as shown in Fig. 14. As shown in Table 10, the ratio of the theoretical maximum load using Yield Line Theory to the experimental maximum load was 93 % for slab (SS) and 101 % for slab (SO). The proposed yield line patterns showed agreement with the experimental results.

4.2.2. The enhance in the ultimate load due to additional strengthening around opening

In the two-way R.C. slabs that were both externally and internally strengthened, the crack patterns were similar to those observed in the control slab with an opening (SO), as shown in Fig. 15. The additional load provided by the strengthening around the opening can be calculated as follows:

$$\sum P_{add} \times \delta = \sum M_{add} \times \theta \tag{12}$$

Where: P_{add} = the additional load, δ = the deflection, θ = the angle of rotation of rods passing through two segments of the slab and M_{add} = the additional moment calculated as the following equation

$$\sum M_{add} \times \theta = T_{add} \times (d_{add} - \frac{a}{2}) \tag{13}$$

Where: T_{add} = the additional tensile force, d_{add} = the effective depth due to the increased strengthening

$$T_{add} = A_{s.int} \times f_y \tag{14}$$

In case of additional internal strengthening

$$T_{add} = A_{f.NSM} \times f_f \tag{15}$$

In case of using NSM technique

$$T_{add} = A_{f.EBR} \times f_f \tag{16}$$

In case of using EBR technique

Eq. (13) demonstrates that the additional moment derived from various strengthening techniques, such as internal steel bars, external GFRP rods using the NSM technique, and GFRP sheets applied with the EBR technique intersecting the crack patterns, meets the allowable limits specified by standards. The tensile forces (T_{add}) can be calculated using Eqs. (14–16), based on the strengthening method applied. Table 10 shows the experimental ultimate load values alongside those obtained from the yield line theory. A comparison indicates that the yield line pattern provides safe estimates for the ultimate loads that strengthened slabs with openings can carry. Additionally, the yield line pattern closely matches the experimental crack patterns observed under

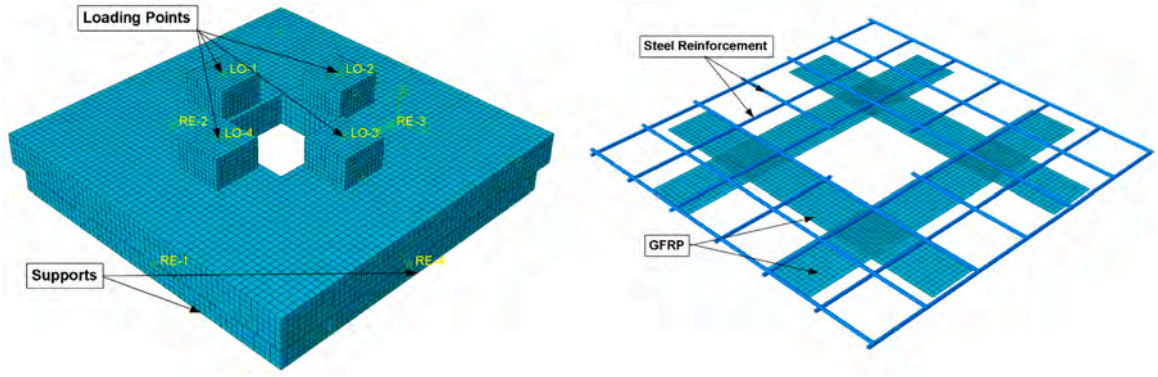

Fig. 16. Finite element model of RC two-way slab.

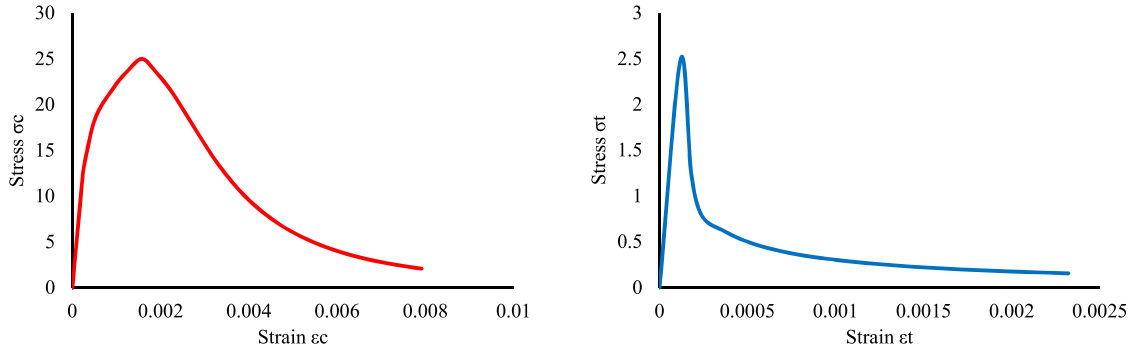

a) Stress-strain behavior of concrete in compression b) Stress-strain behavior of concrete in tension

Fig. 17. Uniaxial stress-strain responses for concrete.

Table 8
Concrete damage plasticity (CDP) parameters.

Parameter	value
Material model	CDP model
Modulus of elasticity E_c – Mpa	22000
Flexural Strength f_r – Mpa	3.58
Tensile strength f_t – Mpa	2.68
Poisson's ratio	0.2
plasticity number – K	2/3
viscosity parameter – μ	0.0001

Table 9
Characteristics of GFRP used in ABAQUS.

Parameters	value
Modulus of elasticity in a longitudinal direction, E1 - GPa	70
Modulus of elasticity in a transverse direction, E2 - GPa	9.5
Longitudinal-transverse Poisson's ratio - Nu12	0.22
Shear modulus, G12, G13, G23 – Mpa	3500
Longitudinal tensile strength – Mpa	2250
Longitudinal Compressive strength – Mpa	2000
Transverse tensile strength – Mpa	50
Transverse compressive strength – Mpa	150
Longitudinal shear strength – Mpa	50
Transverse shear strength – MPa	50

concentrated loading. The increased ultimate load achieved through these strengthening techniques offers a practical and effective solution for structural design.

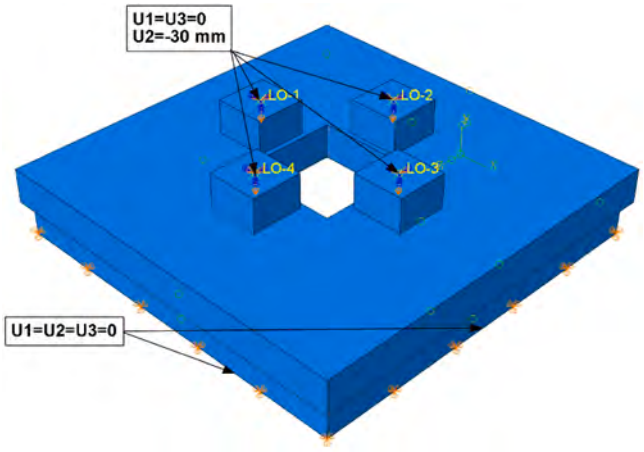

Fig. 18. Load and boundary conditions.

5. Finite element modeling

A 3D nonlinear finite element analysis FEA was carried out to mimic the flexural behavior of two-way R.C. slabs with an opening that were strengthened using various techniques. This process utilized the FEA software ABAQUS/Explicit, version 6.14 [65]. ABAQUS, a highly efficient finite element software, is extensively employed by researchers and engineers for modeling and analyzing complex engineering issues. Fig. 16 illustrates the representation of the RC slab. Ten different RC slab models were analyzed using numerical methods. The model took into account geometric and material nonlinearities, including the elastic-plastic stress-strain relationship obtained from experimental data

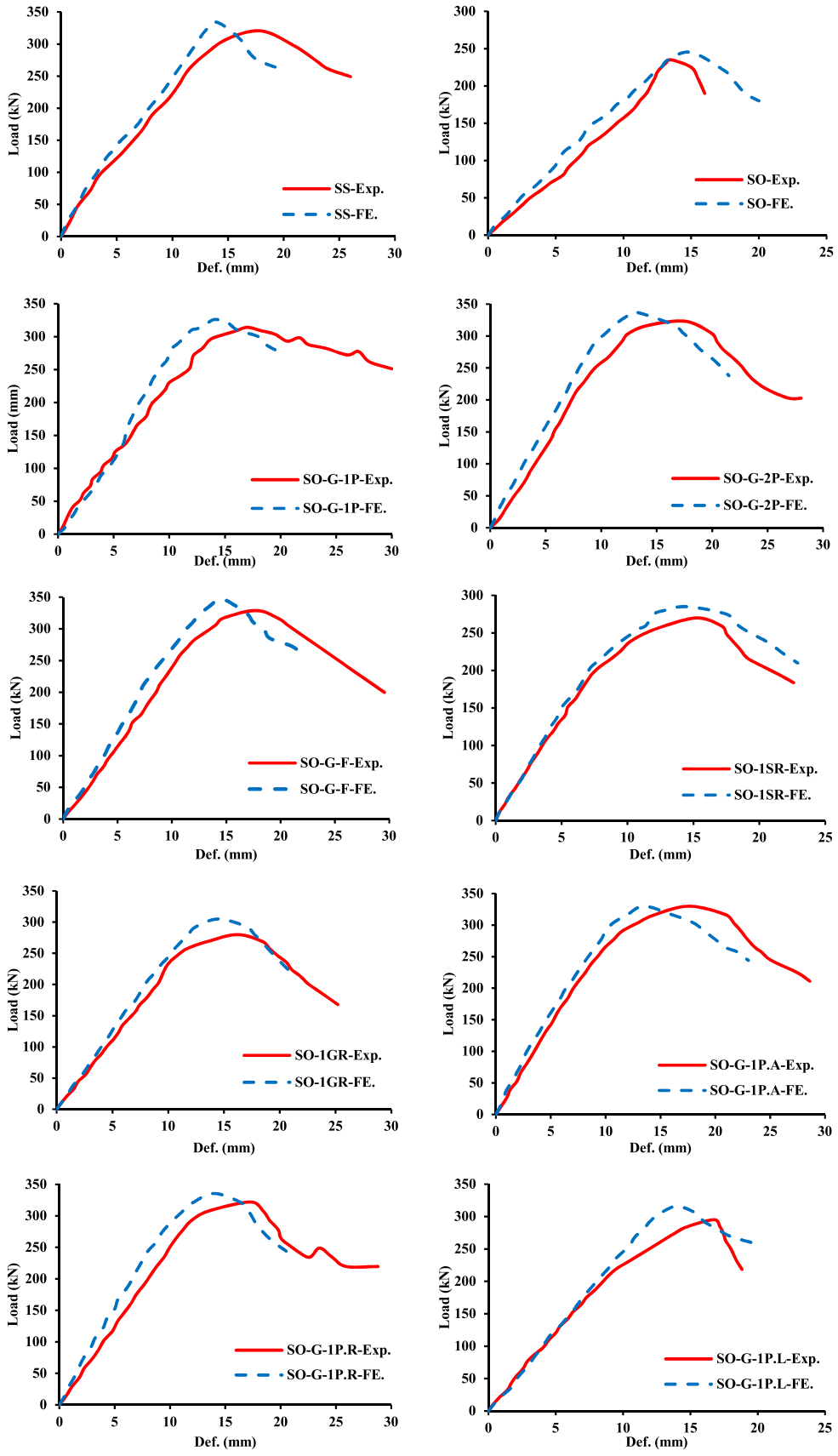

Fig. 19. Comparison between experimental and FE load-deflection curves for all tested slabs.

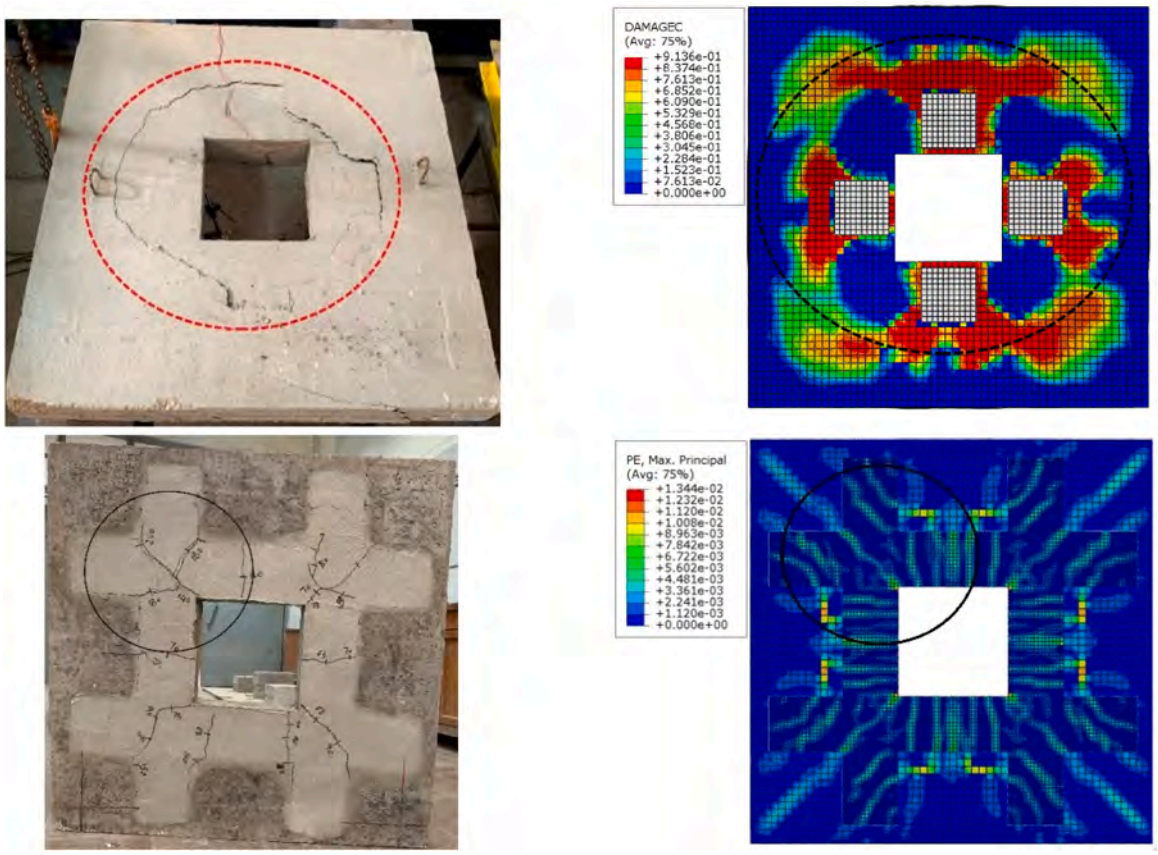

Fig. 20. Comparing experimental cracking patterns to finite element analysis cracking patterns.

for concrete, as shown in Fig. 17. This study examined load-deflection curves, failure mechanisms, and ultimate loads.

5.1. Element type and meshing

All solid components were simulated with C3D8R elements, whereas the GFRP rods and internal steel reinforcement were represented using "truss" elements in all specimen models, and truss sections were simulated using T3D2 elements. The GFRP sheets were modeled as shell elements with a 4-node structure and reduced integration (S4R) with hourglass control. Supports were modeled as rigid regions to ensure uniform force distribution and avoid localized stress concentrations. The mesh refinement was carried out to ensure a uniform distribution of stresses and strains within the concrete core, the GFRP sheet, and the GFRP rods. A mesh convergence study was performed to determine the optimal mesh size for accurate results while minimizing analysis time. In Fig. 16, a fine mesh with 20 mm cube-shaped elements was utilized for the slab in 3D FEA and 15 mm for the GFRP sheet. Internal reinforcement and GFRP rods were meshed at 10 mm and load plates at 15 mm to improve the precision of the FEA results. Nonlinear finite element analysis was conducted using a static general analysis approach based on the Newton-Raphson method. Both the top and bottom surfaces of the slabs had all degrees of freedom unrestricted, and loading was applied using the displacement feature in ABAQUS.

5.2. Material modeling

5.2.1. Concrete

The concrete damaged plasticity model (CDP) was utilized to elucidate how concrete reacts when damaged, aiming to simulate the complete stress-strain characteristics of concrete under compression and tension loads, thereby forecasting its behavior leading up to failure. The overall stress-strain response aligns with concrete's uniaxial compressive and tension behavior within the Concrete Damage Plasticity model (CDP), as depicted in Fig. 17a and b. The yield surface was defined by: Dilation Angle (ψ): Set to 39° to model realistic plastic flow behavior. Biaxial-to-Uniaxial Strength Ratio (fb0/fc0): Set to 1.35, representing typical concrete performance under multiaxial stress. Eccentricity (e): A small value (0.12) was chosen for numerical stability. Failure in compression was defined by the ultimate compressive strain, incorporating crushing damage in the post-peak region. Tensile failure was modeled based on crack formation and propagation, with stiffness degradation implemented to simulate the loss of load-carrying capacity. Table 8 shows the parameters chosen for the "CDP" model.

5.2.2. Steel reinforcement

The steel material was represented using a three-dimensional Von Mises stress criteria-based law of elastoplastic behavior with isotropic hardening. The Von Mises yield criterion was adopted to model the isotropic elastic-plastic behavior of reinforcement bars, incorporating strain hardening for accurate post-yield simulations. The steel properties included a modulus of elasticity (Es) of 210,000 MPa, yield stress (σe) of 574 MPa, plastic strain at yield stress (εp) of 0, ultimate stress (σf) of 742 MPa, and plastic strain at ultimate stress (εp) of 0.0536, as determined in the experimental study. A Poisson's ratio (υ) of 0.3 was assumed for the steel reinforcement. These parameters were used in the Finite Element Model (FEM). Failure occurred when the reinforcement bars reached the ultimate tensile strain defined by experimental data.

5.2.3. GFRP bars

The GFRP rods were simulated in ABAQUS assuming they exhibit isotropic linear elastic behavior, with no damage criteria utilized. It is significant to recognize that the GFRP rods remain linearly elastic until they reach failure.

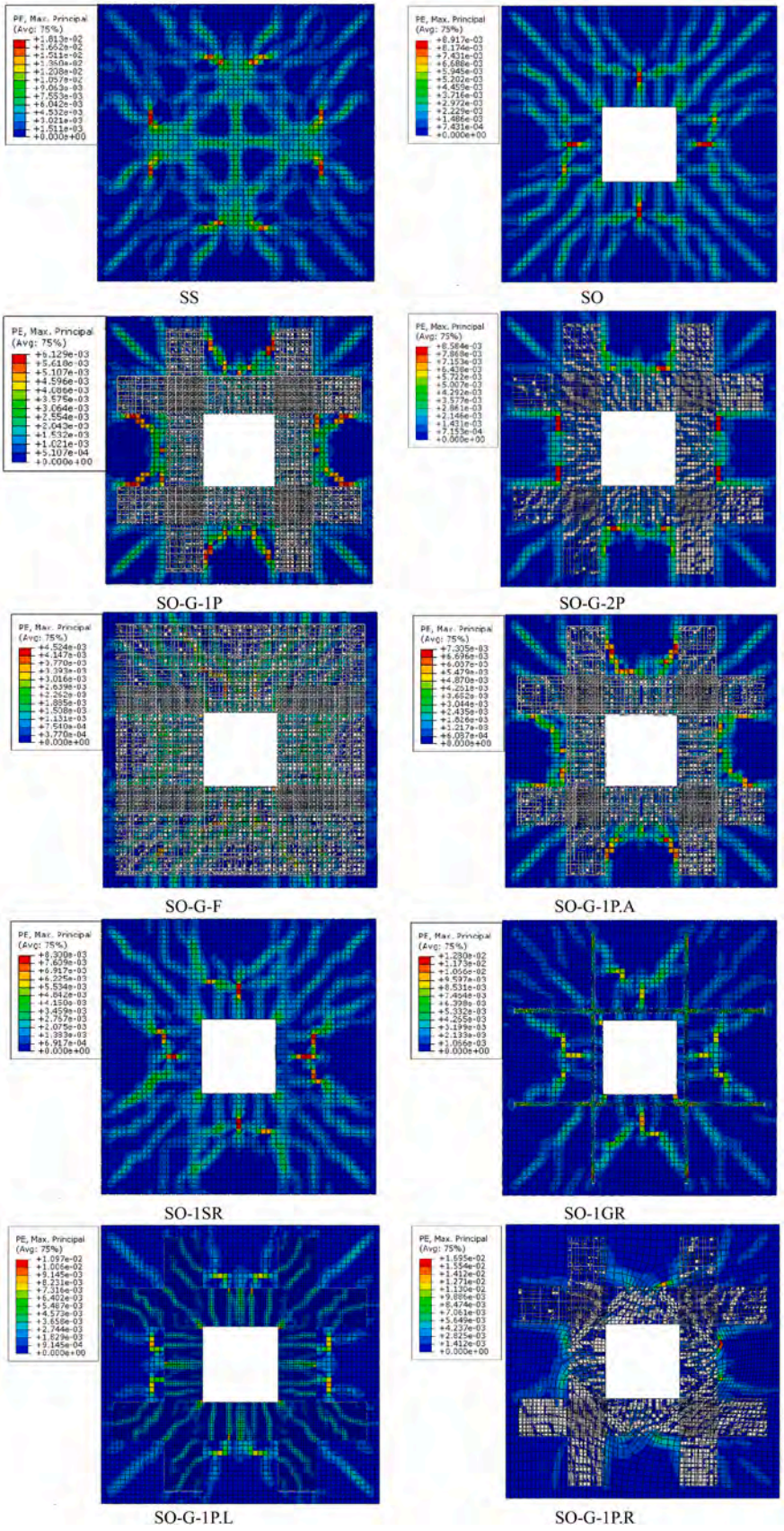

Fig. 21. FE cracks of all tested specimens.

Table 10
Comparison of outcomes obtained from experimental, finite element analysis, and theoretical.

Specimens ID	Failure Load - kN			Theo. Yield Line		$P_{u,\ FE.}/P_{u,\ Exp.}$	$P_{u,\ Th.\ ACI.}/P_{u,\ Exp.}$	$P_{u,\ Y.L.}/P_{u,\ Exp.}$
	Expe.	F. E	Theo. ACI	P_{add}	P_{total}			
SS	320	334	313	——	297	1.04	0.98	0.93
SO	235	245	220	——	237	1.04	0.93	1.01
SO-G-F	329	347	310	165	402	1.05	0.94	1.28
SO-G-1P	314	326	288	76	313	1.04	0.92	0.97
SO-G-2P	323	337	298	152	389	1.04	0.92	1.18
SO-G-1P.A	330	330	N/A	76	313	1.00	N/A	1.16
SO-G-1P.R	322	335	N/A	76	313	1.04	N/A	1.12
SO-G-1P.L	295	315	269	68	306	1.07	0.91	0.93
SO−1GR	280	305	283	137	374	1.09	1.01	1.16
SO−1SR	270	285	279	119	356	1.06	1.03	1.21

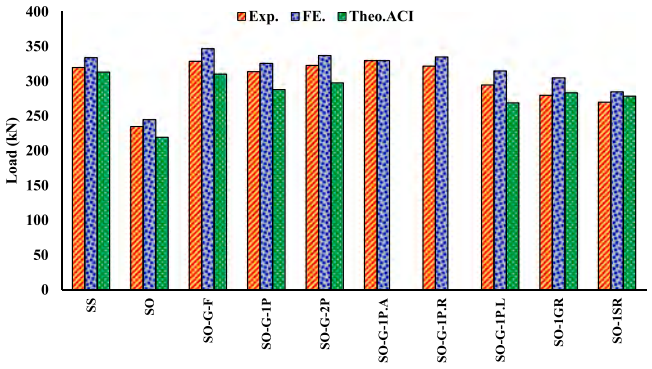

Fig. 22. Comparison of the ultimate load of the experimental, theoretical, and FE results.

5.2.4. GFRP sheets

The GFRP sheets were designed to have orthotropic elastic materials in their structure. To represent these properties in simulations, the material type "LAMINA" was utilized. The elastic modulus in the hoop direction (E1) was determined to be 70 GPa as provided by the manufacturer, considering the different elastic modulus in the transverse and longitudinal directions as well as the shear modulus [66]. The Hashin damage model was employed to simulate the plastic behavior of the GFRP sheets. Table 9 outlines the elastic properties of the material and the various parameters essential for constructing the Hashin damage model.

5.3. Interaction between elements

Utilizing the embedded element constraint in the ABAQUS program allows for accurate modeling of the interaction between concrete and steel reinforcement to ensure a strong bond. The steel reinforcement is considered the embedded region, while the concrete is the host region. Hard contact behavior and tie constraints are used to model the contact between support surfaces and the concrete. A cohesive surface is utilized to simulate the interaction between GFRP and concrete at the interface, accurately modeling the local interface behavior and tension-side strengthening. The "traction separation approach" describes relative displacement at each contact point, with a bi-linear type representing damage evolution and linear elastic behavior up to maximum stresses.

5.4. Load and boundary conditions

The same boundary conditions and loading were used in both the FEA model and the experimental test. The supports were fixed to prevent vertical movement and rotation about the z-axis. The slab section at the support regions was not restrained laterally in the x-direction. A displacement control technique was used to apply the load at four points on the top surface, in the middle of the edges of the opening. A coupling constraint model was used to connect the surface to a reference point to evenly distribute the vertical displacement and avoid localized stress failure. The boundary conditions and applied load were illustrated in Fig. 18, highlighting the restrained and unrestrained regions and the loading locations. This alignment of experimental and numerical conditions enhances the reliability of the FEA model in predicting the structural behavior of the RC slabs with openings.

5.5. Consideration of moderate slab thickness

The effective span-to-thickness ratio (span/h) of approximately 10 categorizes the slabs as having a moderate thickness, bridging the behavior of thin and thick slabs. To address this in the FEM analysis, the Mindlin-Reissner Plate Theory was employed, as it accounts for transverse shear deformation effects. Shell elements with reduced integration were used to model flexural and shear behavior, complemented by solid elements in regions of high stress. These considerations ensured an accurate representation of the combined flexural and shear behavior characteristic of such slabs.

5.6. Comparing the experimental and finite element results

Fig. 19 illustrates the load-deflection relationships for the Finite Element (FE) model and the corresponding experimental findings. Fig. 20 displays a comparison of the cracking patterns observed in experiments and in the FE analysis. Fig. 21 presents the final fractures of the tested slabs using the CDP model. Table 10 and Fig. 22 present the ultimate load and mid-span deflection values derived from the FE analysis, including a comparison with the experimental data. These findings indicate a close alignment between the experimental results and the predictions made by the nonlinear FE models, with minor deviations. The use of the CDP model demonstrates a robust correlation between the anticipated FE results and the experimental outcomes, with the failure load variance falling within the 0–9 percent range. This study reveals that employing the CDP model, which primarily relies on the concept of damaged concrete, to establish parameter values for describing concrete behavior leads to more precise results, consistent with previous simulation studies.

6. Parametric studies

A parametric analysis is developed and executed in this study to expand knowledge and evaluate the effects of various parameters on the structural behavior of two-way reinforced concrete slabs with openings. The variables considered in the parametric study include the shape of the cutout (circular, octagonal, and rectangular), the strengthening length (1000 mm or 600 mm), and the rod end configuration (straight or hooked). Samples SS and SO are designated as the reference slabs for this analysis.

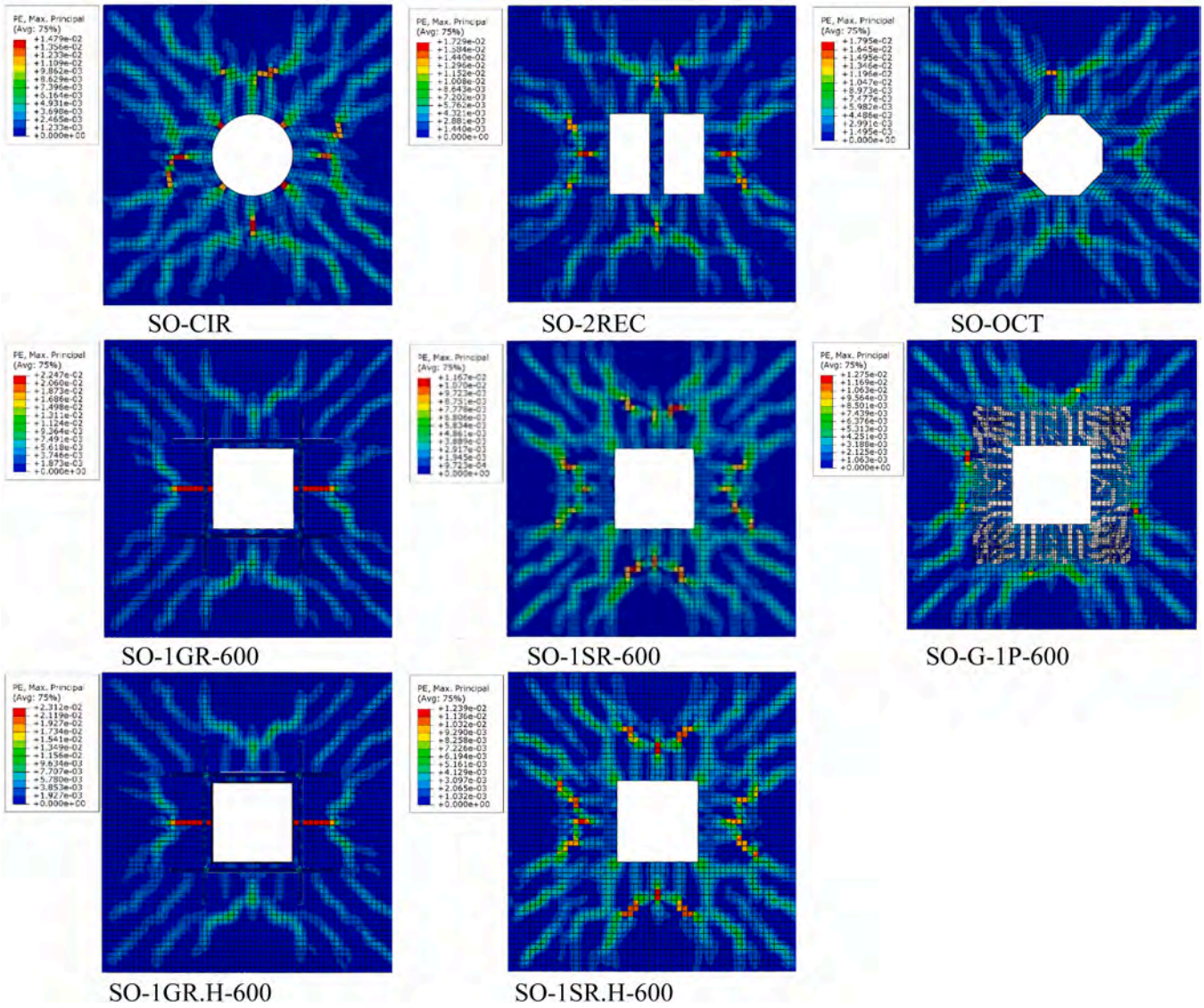

Fig. 23. FE cracks for all specimens from the parametric studies.

6.1. *Influence of cutout shape*

This study investigated how cut-out shape influences two-way R.C. slabs' flexural performance. Finite element models (SO-CIR), (SO-OCT), and (SO-2REC) were created with circular, octagonal, and double-rectangular cut-outs, respectively. Crack patterns for these models are shown in Fig. 23. Changing the cut-out shape increased the load-carrying capacity by 2 %, 1 %, and 6 %, respectively, and mid-span deflections by 2 %, 1 %, and 4 % compared to the reference model (SO). Fig. 24 presents the load-deflection responses for these slabs.

6.2. *Effect of strengthening length*

The effect of varying strengthening lengths was investigated on three specimens: (SO-1GR-600), (SO-1SR-600), and (SO-G-1P-600). These specimens were strengthened using a 600 mm NSM GFRP bar, a 600 mm internal steel bar, and a 600 mm EBR GFRP strip, respectively. The results were compared with those of experimentally tested specimens, (SO-1GR), (SO-1SR), and (SO-G-1P), which were strengthened with 1000 mm reinforcement lengths. Fig. 23 illustrates the crack patterns observed in the specimens. Increasing the strengthening length resulted in a slight enhancement in the load-carrying capacity of the slabs, with increases ranging from 2 % to 6 % in capacity and 1–3 % in mid-span deflection compared to the slabs strengthened with 600 mm lengths. Fig. 24 presents the corresponding load-deflection curves for the specimens.

6.3. *Effect of rod end configuration*

The impact of rod end configurations on the structural performance of two specimens, (SO-1GR.H-600) and (SO-1SR.H-600), was investigated. These specimens were strengthened using 600 mm GFRP rods with hooked ends (NSM technique) and 600 mm internal steel bars with hooked ends. The results were compared to those of specimens (SO-1GR-600) and (SO-1SR-600), which were strengthened with straight-end rods. Fig. 23 illustrates the observed crack patterns in the specimens. The inclusion of hooks at the ends of the strengthening bars resulted in a significant improvement in the slabs' load-carrying capacity. The load-carrying capacity increased by 7–13 %, and deflection increased by 4–9 % when compared to the specimens with straight-end strengthening. Fig. 24. presents the corresponding load-deflection curves for the specimens.

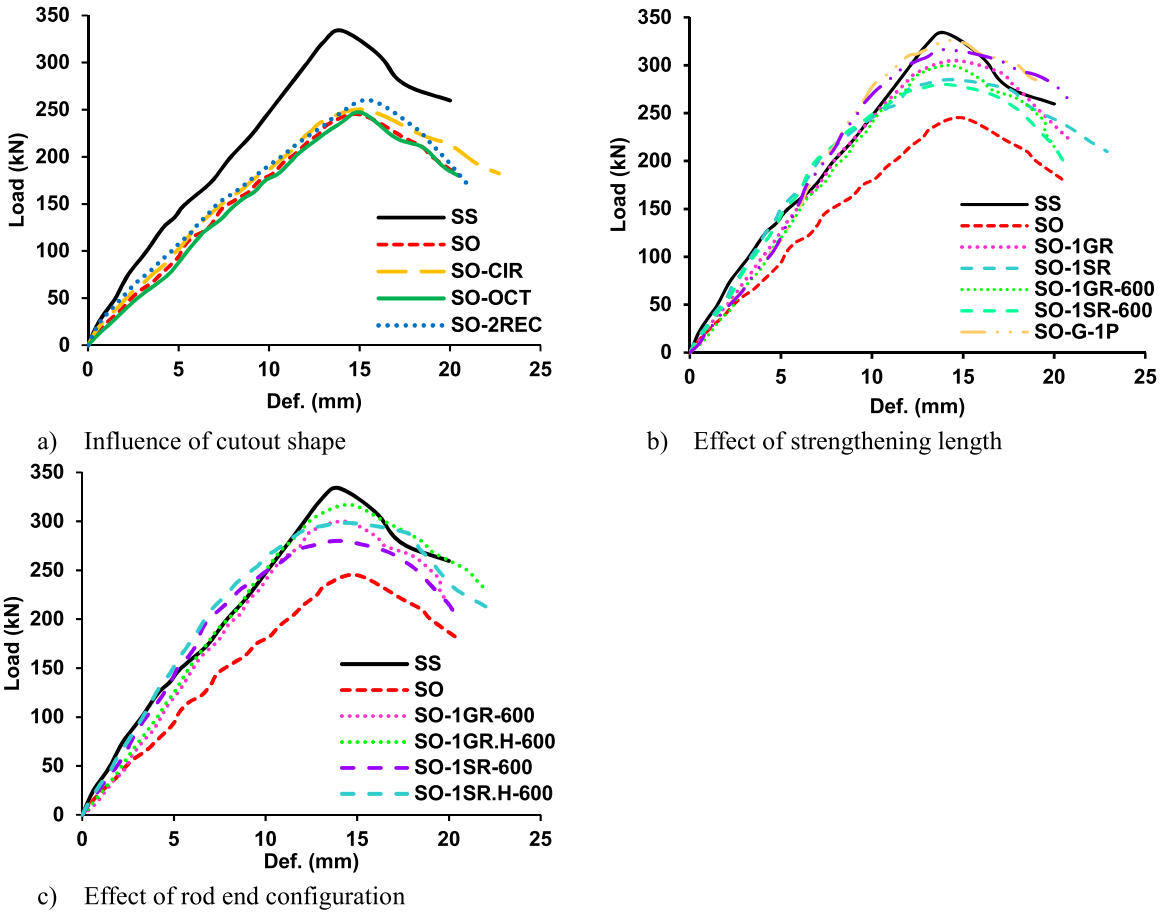

Fig. 24. Load-deflection curves for all (FE) specimens from the parametric studies.

7. Conclusions

This study analyzed the flexural behavior of two-way reinforced concrete (RC) slabs with openings strengthened with glass fiber-reinforced polymer (GFRP) sheets and rods using various techniques. The slabs were analyzed to assess their structural performance when subjected to four-point loads. The experimental results were assessed, specifically examining the causes of cracking and failure, the response of deflection, and the ultimate capacity. Below are the conclusions obtained through this research.

- An opening that occupies 12 % of the slab area, particularly in the center of the slab spans, influences the performance of two-way slabs significantly. This opening resulted in a 36 % decrease in the slabs' load-carrying capacity.
- In slabs strengthened by EB-GFRP, the bonding between the concrete and GFRP sheets affects the strength of the slabs, so it is recommended to use anchors with the EB-GFRP technique.
- The addition of anchors to GFRP sheets in slab SO-G-1P.A. resulted in a 40 % increase in ultimate load capacity compared to the reference slab with an opening. This increase was attributed to the increased bonding between the GFRP sheets and the concrete surface, as the slab collapsed due to punching shear, but did not collapse due to debonding.
- In slab SO-G-1P.L., the addition of a layer to the concrete surface resulted in a significant increase in ductility, with an 81 % improvement compared to the reference slab with an opening. This improvement can be attributed to the early appearance of cracks caused by the separation between the new layer and the concrete surface.
- The finite element (FE) results exhibit good agreement with the experimental results for the maximum loads of the tested slabs, the pattern of cracks, and the deflection at the maximum load. It suggests that most of the established criteria and methods used to depict the qualities, interactions, and limitations of the materials were almost sufficiently accurate to pave the way for future studies, parametric studies, and investigations.
- Theoretical and empirical models exhibited a good degree of concordance. The average $P_{Theror.}/P_{Exp.}$ ratio of all slabs ranged from 0.92 to 1.03.
- Double-rectangular cut-outs showed the highest performance, achieving a 6 % increase in load-carrying capacity and a 4 % rise in mid-span deflection compared to circular and octagonal shapes. Compared to the other configurations, the formation of the opening cut off fewer reinforcement bars, leading to this improved behavior.
- Hooked-end rods significantly enhanced performance, increasing load-carrying capacity by 7–13 % and mid-span deflection by 4–9 %. This improvement is due to the increased bond between the concrete and the strengthening rods.

8. Limitation of the study

The study's limitations include the following:

- Scale and Boundary Conditions: Experiments were conducted on scaled-down slabs under idealized boundary conditions, which may not fully replicate real-world scenarios or large-scale applications.
- Environmental Exclusions: Laboratory testing did not account for environmental factors like temperature changes, humidity, or chemical exposure, limiting insights into long-term durability.

- Economic Feasibility: Practical implementation challenges, such as cost-effectiveness and ease of installation, were not thoroughly evaluated.

Future research should address these gaps by incorporating large-scale testing, real-world conditions, and economic evaluations.

9. Future research direction

In this study, we propose several future research directions to enhance the application of strengthening techniques for RC slabs with openings. One area of focus is investigating the impact of larger openings on load-carrying capacity and deflection control, along with analyzing the effects of different shapes and positions of openings on structural performance. Another critical aspect involves examining the optimal design and placement of mechanical anchors to enhance the bond strength between FRP and concrete. Furthermore, advanced strengthening methods, such as hybrid fiber-reinforced polymers (FRPs), ultra-high-performance concrete (UHPC), and textile-reinforced mortar (TRM), should be explored to achieve improved mechanical performance and durability. Future research should also focus on evaluating the behavior of strengthened slabs under extreme conditions, assessing the cost-effectiveness of various strengthening techniques, and exploring sustainable solutions, such as recycled FRPs and low-carbon concrete, to minimize environmental impact.

CRediT authorship contribution statement

Khaleel Gamal I.: Writing – review & editing, Supervision, Methodology, Investigation, Conceptualization. **AbdelBaset Mohamed:** Writing – original draft, Methodology, Investigation, Data curation. **Bondok Marwa H.:** Writing – original draft, Validation, Investigation, Formal analysis, Data curation. **Makhlouf Mohamed H.:** Writing – review & editing, Validation, Supervision, Methodology, Investigation, Conceptualization.

Declaration of Competing Interest

The authors declare that they have no known competing financial interests or personal relationships that could have appeared to influence the work reported in this paper.

References

[1] Afefy HM, Fawzy TM. Strengthening of RC one-way slabs including cut-out using different techniques. Eng Struct 2013;57:23–36. https://doi.org/10.1016/j.engstruct.2013.09.013.

[2] Al-Hafiz Ali M, Chiad Salam S, Farhan Mohannad S. Flexural strength of reinforced concrete one-way opened slabs with and without strengthening. Aust J Basic Appl Sci 2013;7:642–51.

[3] Anil Ö, Kaya N, Arslan O. Strengthening of one way RC slab with opening using CFRP strips. Constr Build Mater 2013;48:883–93. https://doi.org/10.1016/j.conbuildmat.2013.07.093.

[4] Khalil AEA, Atta AM, Hassan A, Abd-Elaaty AH. Flexural strength recovery of RC one-way slabs having cut-outs using NSM-SHCC plates. Eng Struct 2022;258. https://doi.org/10.1016/j.engstruct.2022.114149.

[5] Smith ST, Kim SJ. Strengthening of one-way spanning RC slabs with cutouts using FRP composites. Constr Build Mater 2009;23:1578–90. https://doi.org/10.1016/j.conbuildmat.2008.06.005.

[6] H.M. Seliem, E.A. Sumner, R. Seracino, S.T. Smith, Field testing of RC slabs with openings strengthened with CFRP, in: Fourth International Conference on FRP Composites in Civil Engineering (CICE2008), Zurich, Switzerland, 2008.

[7] Vasquez Alvaro, Karbhari Vistasp M. Fiber-reinforced polymer composite strengthening of concrete slabs with cutouts. Acids Struct J 2003;100:665–73. https://doi.org/10.14359/12808.

[8] Tan KH, Zhao H. Strengthening of openings in one-way reinforced-concrete slabs using carbon fiber-reinforced polymer systems. J Compos Constr 2004;8:393–402. https://doi.org/10.1061/(ASCE)1090-0268(2004)8:5(393).

[9] A.A. Elsayed, N. Amer, Experimental Analysis of Centrally Opened Two-Way Slabs Strengthened With Carbon Fiber Laminates, 2015.

[10] Floruţ SC, Sas G, Popescu C, Stoian V. Tests on reinforced concrete slabs with cut-out openings strengthened with fibre-reinforced polymers. Compos B Eng 2014;66:484–93. https://doi.org/10.1016/j.compositesb.2014.06.008.

[11] Ridah AA, Al-Fatlawi S, Abed A. CFRP strengthening of concrete slabs with and without openings. Int J Sci Technol Res 2015;4:8. ⟨www.ijstr.org⟩.

[12] S.J. Kim, S.T. Smith, STRENGTHENING OF RC SLABS WITH LARGE PENETRATIONS USING ANCHORED FRP COMPOSITES, n.d.

[13] El-Mawsly EH, El-Kashif KFO, Shawky AA, Abdalla HA. Experimental and numerical investigation on strengthening of RC flat slabs with central opening. Case Stud Constr Mater 2022;16. https://doi.org/10.1016/j.cscm.2022.e00974.

[14] Aman SS, S. Mohammed B, Wahab MA, Anwar A. Performance of reinforced concrete slab with opening strengthened using CFRP. Fibers 2020;8. https://doi.org/10.3390/fib8040025.

[15] S. Badawy, M. Elsayed, A. Elsayed, Using Ferrocement Laminates in Strengthening Flexural Behavior of R.C. Slabs with Opening, 2015. ⟨http://www.lifesciencesite.comhttp://www.lifesciencesite.com.17⟩.

[16] Choi Y, Park IH, Kang SG, Cho CG. Strengthening of RC slabs with symmetric openings using GFRP composite beams. Polymers 2013;5:1352–61. https://doi.org/10.3390/polym5041352.

[17] Ashteyat AM, Al Rjoub YS, Obaidat AT, Dagamseh H. Strengthening and repair of one-way and two-way self-compacted concrete slabs using near-surface-mounted carbon-fiber-reinforced polymers. Adv Struct Eng 2019;22:2435–48. https://doi.org/10.1177/1369433219843649.

[18] El-Mandouh MA, Elsamak G, O. Rageh B, Hamoda A, Abdelazeem F. Experimental and numerical investigation of one-way reinforced concrete slabs using various strengthening systems. Case Stud Constr Mater 2023;18. https://doi.org/10.1016/j.cscm.2022.e01691.

[19] Aljidda O, El Refai A, Alnahhal W. Experimental and numerical investigation of the flexural behavior of one–way RC slabs strengthened with near–surface mounted and externally bonded systems. Constr Build Mater 2024;421. https://doi.org/10.1016/j.conbuildmat.2024.135709.

[20] Zhou C, Wang L, Wang Y, Fang Z. Experimental study on the flexural strengthening of one-way RC slabs with end-buckled and/or externally bonded CFRP sheets. Eng Struct 2023;282. https://doi.org/10.1016/j.engstruct.2023.115832.

[21] Aljidda O, Alnahhal W, El Refai A. Flexural strengthening of one-way reinforced concrete slabs using near surface-mounted BFRP bars. Eng Struct 2024;303. https://doi.org/10.1016/j.engstruct.2024.117507.

[22] D. Banu, N. Ţăranu, R. Carneiro De Barros, P. Ciobanu, S. Popoaei, D. Banu, N. Ţăranu, R.C. Barros, P. Ciobanu, S. Popoaei, EXPERIMENTAL STUDY OF TWO WAY RC SLABS WITH OR WITHOUT OPENINGS STRENGTHENED WITH COMPOSITE STRIPS B. EXPERIMENTAL RESULTS, n.d.

[23] A.S. Mosallam, K.M. Mosalam, Strengthening of two-way concrete slabs with FRP composite laminates, 2003.

[24] Türer A, Mercimek Ö, Anıl Ö, Erbaş Y. Experimental and numerical investigation of punching behavior of two-way RC slab with different opening locations and sizes strengthened with CFRP strip. Structures 2023;49:918–42. https://doi.org/10.1016/j.istruc.2023.01.157.

[25] Al-Azzawi AA, Mtashar SH. Behavior of two-way reinforced concrete voided slabs enhanced by steel fibers and GFRP sheets under repeated loading. Results Eng 2023;17. https://doi.org/10.1016/j.rineng.2022.100872.

[26] Mahlis M, Shoeib AE, Abd Elnaby S, Sherif A. The Effect of Cutting Openings on the Behavior of Two-way Solid Loaded Slabs. Structures 2018;16:137–49. https://doi.org/10.1016/j.istruc.2018.09.002.

[27] Labibzadeh M, Elahifar T. An enhanced finite element model for reinforced concrete two-way slabs strengthened with carbon fiber reinforced polymers. Struct Eng Int 2015;25:81–90. https://doi.org/10.2749/101686614X14043795570093.

[28] Eskandarinadaf A, Reza Esfahani M. Strengthening of two-way RC slabs with central opening. KSCE J Civ Eng 2019;23:1228–35. https://doi.org/10.1007/s12205-019-0952-y.

[29] Hamad AG, Mohamad Ali AA. Strengthening of self-compacted concrete two way slabs with opening using near surface mounted (NSM) fiber reinforced polymers (FRP) technique. IOP Conf Ser Mater Sci Eng. IOP Publishing Ltd; 2020. https://doi.org/10.1088/1757-899X/928/2/022148.

[30] Enochsson O, Lundqvist J, Täljsten B, Rusinowski P, Olofsson T. CFRP strengthened openings in two-way concrete slabs - an experimental and numerical study. Constr Build Mater 2007;21:810–26. https://doi.org/10.1016/j.conbuildmat.2006.06.009.

[31] Al-Rousan R. Influence of opening sizes on the flexural behavior of heat-damaged reinforced concrete slabs strengthened with CFRP ropes. Case Stud Constr Mater 2022;17. https://doi.org/10.1016/j.cscm.2022.e01464.

[32] Türer A, Mercimek Ö, Anıl Ö, Erbaş Y. Experimental and numerical investigation of punching behavior of two-way RC slab with different opening locations and sizes strengthened with CFRP strip. Structures 2023;49:918–42. https://doi.org/10.1016/j.istruc.2023.01.157.

[33] Bonaldo E, de Barros JA, Lourenço PB. Efficient strengthening technique to increase the flexural resistance of existing RC slabs. J Compos Constr 2008;12:149–59. https://doi.org/10.1061/(ASCE)1090-0268(2008)12:2(149).

[34] J.E. Bolander, S. Berton, Simulation of shrinkage induced cracking in cement composite overlays, (n.d.). ⟨https://doi.org/10.1016/j.cemconcomp.2003.04.002⟩.

[35] Barros JAO, Cunha VMCF, Ribeiro AF, Antunes JAB. Post-cracking behaviour of steel fibre reinforced concrete. Mater Struct Mater Et Constr 2005;38:47–56. https://doi.org/10.1617/14058.

[36] Walser R, Steiner W. Strengthening a bridge with advanced materials. Struct Eng Int 1997;7:110–2. https://doi.org/10.2749/101686697780495094.

[37] Almassri B, Halahla AM. Corroded RC beam repaired in flexure using NSM CFRP rod and an external steel plate. Structures 2020;27:343–51. https://doi.org/10.1016/j.istruc.2020.05.054.
[38] Arslan G, Sevuk F, Ekiz I. Steel plate contribution to load-carrying capacity of retrofitted RC beams. Constr Build Mater 2008;22:143–53. https://doi.org/10.1016/j.conbuildmat.2006.10.009.
[39] Su RKL, Zhu Y. Experimental and numerical studies of external steel plate strengthened reinforced concrete coupling beams. Eng Struct 2005;27:1537–50. https://doi.org/10.1016/j.engstruct.2005.04.012.
[40] Teng JG, Smith ST, Yao J, Chen JF. Intermediate crack-induced debonding in RC beams and slabs. Constr Build Mater 2003:447–62. https://doi.org/10.1016/S0950-0618(03)00043-6.
[41] Muciaccia G, Khorasani M, Mostofinejad D. Effect of different parameters on the performance of FRP anchors in combination with EBR-FRP strengthening systems: a review. Constr Build Mater 2022;354. https://doi.org/10.1016/j.conbuildmat.2022.129181.
[42] Abas Golham M, Al-Ahmed AHA. Behavior of GFRP reinforced concrete slabs with openings strengthened by CFRP strips. Results Eng 2023;18. https://doi.org/10.1016/j.rineng.2023.101033.
[43] Dalfré GM, Barros JAO. NSM technique to increase the load carrying capacity of continuous RC slabs. Eng Struct 2013;56:137–53. https://doi.org/10.1016/j.engstruct.2013.04.021.
[44] Pachalla SKS, Prakash SS. Efficient near surface mounting CFRP strengthening of pretensioned hollowcore slabs with opening – an experimental study. Compos Struct 2017;162:28–38. https://doi.org/10.1016/j.compstruct.2016.11.072.
[45] Limam O, Foret G, Ehrlacher A. RC two-way slabs strengthened with CFRP strips: experimental study and a limit analysis approach. Compos Struct 2003;60:467–71. https://doi.org/10.1016/S0263-8223(03)00011-4.
[46] Correia L, Teixeira T, Michels J, Almeida JAPP, Sena-Cruz J. Flexural behaviour of RC slabs strengthened with prestressed CFRP strips using different anchorage systems. Compos B Eng 2015;81:158–70. https://doi.org/10.1016/j.compositesb.2015.07.011.
[47] Vijayan DS, Sivasuriyan A, Devarajan P, Stefańska A, Wodzyński Ł, Koda E. Carbon fibre-reinforced polymer (CFRP) composites in civil engineering application—a comprehensive review. Buildings 2023;13. https://doi.org/10.3390/buildings13061509.
[48] Yoo DY, Banthia N, Yoon YS. Recent development of innovative steel fibers for ultra-high-performance concrete (UHPC): a critical review. Cem Concr Compos 2024;145. https://doi.org/10.1016/j.cemconcomp.2023.105359.
[49] El-Hacha Raafat, Rizkalla Sami H. Near-surface-mounted fiber-reinforced polymer reinforcements for flexural strengthening of concrete structures. Acids Struct J 2004;101:717–26. https://doi.org/10.14359/13394.
[50] T. Triantafillou, S. Matthys, K. Audenaert, G. Balázs, M. Blaschko, H. Blontrock, C. Czaderski, E. David, A. Di Tomasso, W. Duckett, D. Hordijk, M. Leeming, H. Meier, G. Monti, R. Moss, U. Neubauer, R. Niedermeier, B. Taljsten, G. Zehetmaier, K. Zilch, fib Bulletin 14. Externally bonded FRP reinforcement for RC structures, fib. The International Federation for Structural Concrete, 2001. ⟨https://doi.org/10.35789/fib.BULL.0014⟩.
[51] Hassan T, Rizkalla S. Investigation of bond in concrete structures strengthened with near surface mounted carbon fiber reinforced polymer strips. J Compos Constr 2003;7:248–57. https://doi.org/10.1061/(ASCE)1090-0268(2003)7:3(248).
[52] De Lorenzis L, Teng JG. Near-surface mounted FRP reinforcement: an emerging technique for strengthening structures. Compos B Eng 2007;38:119–43. https://doi.org/10.1016/j.compositesb.2006.08.003.
[53] T.Q. Syed Shah, An Alternative Strengthening Technique using a Combination of FRP Sheets and Rods to Improve Flexural Performance of Continuous RC Slabs, (2016). ⟨http://rave.ohiolink.edu/etdc/view?acc_num=toledo1469151846⟩ (accessed December 15, 2024).
[54] K.H. Mahfuz, U.D. Darain, STRENGTHENING PERFORMANCE OF REINFORCED CONCRETE BEAM USING COMBINED EXTERNALLY BONDED AND NEAR SURFACE MOUNTED TECHNIQUES, n.d.
[55] Erdem RT, Gucuyen E. Non-linear analysis of reinforced concrete slabs under impact effect. Gradjevinar 2017;69:479–87. https://doi.org/10.14256/JCE.1557.2016.
[56] Tuğrul Erdem R, Berberoğlu M, Gücüyen E. Investigation of concrete slabs made with cement based mortars under impact loads. Gradjevinar 2023;75:117–27. https://doi.org/10.14256/JCE.3159.2021.
[57] Qsymah A, Ayasrah M. Finite element analysis of two-way reinforced concrete slabs strengthened with FRP under flexural loading. Buildings 2024;14:3389. https://doi.org/10.3390/buildings14113389.
[58] Erdem RT. Dynamic responses of reinforced concrete slabs under sudden impact loading. Rev De La Construccion 2021;20:346–58. https://doi.org/10.7764/RDLC.20.2.346.
[59] American Concrete Institute. ACI Committee 440., Guide for the design and construction of externally bonded FRP systems for strengthening concrete structures. American Concrete Institute; 2017.
[60] British Standards Institution. Testing hardened concrete. Part 3, Compressive strength of test specimens. BSI; 2002.
[61] Egyptian code for design and construction of reinforced concrete structures (ECP 203-2020), 2020.
[62] Soltani H, Khaloo A, Sadraie H. Dynamic performance enhancement of RC slabs by steel fibers vs. externally bonded GFRP sheets under impact loading. Eng Struct 2020;213. https://doi.org/10.1016/j.engstruct.2020.110539.
[63] Jihad A, Rami H, Aghajan J, Lecturer S, Candidate P. Flexural and Flexural Toughness of Fiber Reinforced Concrete-American Standard Specifications Review. GRD J Eng 2019;4. ⟨www.grdjournals.com⟩.
[64] American Concrete Institute; 2019. https://doi.org/10.14359/51716937. 318-19 Building Code Requirements for Structural Concrete and Commentary.
[65] ABAQUS Analysis User's Manual, 2014.
[66] Hany NF, Hantouche EG, Harajli MH. Finite element modeling of FRP-confined concrete using modified concrete damaged plasticity. Eng Struct 2016;125:1–14. https://doi.org/10.1016/j.engstruct.2016.06.047.